University of Reading

School of Mathematical and Physical Sciences

The Earth's Atmospheric Angular Momentum Budget and its Representation in Reanalysis Observation Datasets and Climate Models

Simon Driscoll

August 2010

This dissertation is a joint MSc in the Departments of Mathematics and Meteorology and is submitted in partial fulfilment of the requirements for the degree of Master of Science

Acknowledgements

I acknowledge the modelling groups, the Program for Climate Model Diagnosis and Intercomparison (PCMDI) and the World Climate Research Programme's (WCRP's) Working Group on Coupled Modelling (WGCM) for their roles in making available the WCRP CMIP3 multi-model dataset. Support of this dataset is provided by the Office of Science, U.S. Department of Energy.

20th Century Reanalysis data is provided by the NOAA/OAR/ESRL PSD, Boulder, Colorado, USA, from their website at http://www.esrl.noaa.gov/psd/

Support for the Twentieth Century Reanalysis Project dataset is provided by the U.S. Department of Energy, Office of Science Innovative and Novel Computational Impact on Theory and Experiment (DOE INCITE) program, and Office of Biological and Environmental Research (BER), and by the National Oceanic and Atmospheric Administration Climate Program Office.

I would very much like to thank the Natural Environment Research Council (NERC) for funding my MSc with an NERC Studentship, all the teamakers who's wonderful products have fuelled ideas throughout this project, and last, but not least, my supervisor: Valerio Lucarini. Mille grazie!

Declaration

I confirm that this is my own work and the use of all material from other sources has been properly and fully acknowledged

Signed:.....

Simon Driscoll

Abstract

Angular Momentum is a fundamental quantity in any rotating system. In this dissertation we are predominantly concerned with the theory of conservation of angular momentum in the Earth's Atmosphere, and whether this theory is represented in the National Oceanic and Atmospheric Administration's (NOAA's) Twentieth Century Reanalysis Version 2 Observation Dataset, the Hadley Centre's HadCM3 and HadGEM1 climate models, and the NOAA's GFDL CM2.0 climate model. By doing this we gain useful information as to whether the reanalysis observation dataset has internally consistent physics after the data assimilation process and the parameterization of variables, and we can also gain useful information as to whether a climate model (that does not require the data assimilation phase) has correct parametrizations of variables and internally consistent physics.

We find that the NOAA Reanalysis Observation Dataset does not conserve angular momentum, and that the torques are the major source of error. There is error in all torques, especially during the northern hemisphere winter. The little change in the latitudinal torque profiles for the reanalysis observation dataset, calculated for 1890-1899 and 1990-1999, suggests that with the aid of the reanalysis process a very poor observation network can give the same latitudinal torque profiles as the observation network of today.

It is also found that the HadCM3 model has a serious error in its representation of the mountain torque, and we note with great interest that the climate model HadGEM1 (who's physical processes were developed from HadCM3) has significantly smaller values in its regional friction torque than that of HadCM3. Indeed all the other latitudinal profiles calculated in this dissertation, implying the surface winds are too weak, and even suggesting there may be differences in the whole circulation between HadGEM1 and HadCM3. We also find error in the spatial patterns of the torques of the NOAA GFDL CM2.0 model whose near symmetric torques imply that the circulation throughout the atmosphere is likely to be symmetric about the equator, thus the northern hemisphere circulation is the same as that of the southern hemisphere in the model.

Contents

List of Figures

Chapter 1

Introduction

There are only a few atmospheric variables that can be used to effectively compare the large scale circulation of the true observed atmosphere and the simulated atmosphere in climate models. Angular Momentum, a fundamental quantity of central importance to the atmosphere, and indeed any rotating system (as mentioned in Egger et al. (2007)), is one of these. The Angular Momentum budget represents a beautiful example of how the atmosphere, oceans and solid earth interact and are inextricably linked through a conservation law (Oort (1989)), and it is of interest to researchers studying any one of these different elements.

Lucarini (2008) points to the need for further confirmation of the basic physical and dynamical processes in climate models, and Peixoto and Oort (2007) note that applying the theory of angular momentum to the climate system can lead to general conclusions about the climate system, which we can use to test both the observed values of the real atmosphere and that of climate models, individually, and in comparisons.

The total angular momentum of the atmosphere, oceans and earth does not change except for a slow secular decrease due to the gravitational force exerted by planets. However, there is transfer between the three components of the earth mentioned above, and if angular momentum increases in the atmosphere it must have been transferred from one of the other elements into the atmosphere, analogously if the atmosphere loses angular momentum it needs to transferred to one of these elements.

In this dissertation we are concerned with the theory of angular momentum in the earth's atmosphere and the torques (the 'turning' or rotational forces) that affect the angular momentum of the atmosphere, and whether the what we discern from the theory can be seen in what is called a 'reanalysis observation dataset' and three state of the art climate models. Reanalysis observation datasets are a literally a re-analyses intended to replace the original analyses observation datasets (literally the recorded quantities of atmospheric variables) because of the need to alleviate many problems that arose from

the original anaylses datasets. Over time there has been a significant improvement in the ability to record accurate data and the results from a continuously improving network of instruments induces an extra time dependent change into the results that is not due to any physical processes. Unsurprisingly, this had a large effect on climate studies and produced changes in the observed climate that were not true, thus reanalysis seeks to improve the old analyses datasets and get rid of this bias. By using state of the art data assimilation to the old data, improving quality control, and by keeping the data assimilation process and computer model used for all the computed results the same, we create a more reliable observation dataset than the original time dependent observation analyses dataset.

This reanalysis dataset is the National Oceanic and Atmospheric Administration's (NOAA's) Twentieth Century Reanalysis Version 2 - a new and rarely studied reanalyis observation dataset. The climate models that we study were used for the fourth assessment report of the Intergovernmental Panel on Climate Change (IPCC), and are The Hadley Centre Global Environmental Model version 1 , or "HadGEM1", the Hadley Centre Coupled Model version 3, or "HadCM3", and the NOAA's Geophysical Fluid Dynamics Laboratory CM2.0 model, or "NOAA GFDL CM2.0". The data from these models is made available through the World Climate Research Programme's (WCRP's) Coupled Model Intercomparison Project phase 3 (CMIP3) multi-model dataset. We first study the theory of angular momentum and its wider links with a central focus on angular momentum conservation, and after this we test the datasets. In doing so we cross the boundaries of numerical approximations, theoretical physics, and computation and modelling.

If a reanalysis observation dataset is consistent with reality, it will, due to the conservation of angular momentum, show that angular momentum of the earth and its atmosphere is conserved. The information gleaned as to whether an observation dataset holds true to the theory of angular momentum tells us something about the data assimilation process and the parameterizations of variables used in the model. Due to the sophistication of the observation network used to record the data, if a reanalysis observation dataset does not conserve angular momentum, then, given that the error in the numerical approximation is smaller than discrepancies seen in the atmosphere's angular momentum budget, the error in the angular momentum conservation will lie in the approximations of data assimilation and the parametrizations involved (a 'parametrization' of a climatic variable is the representation of physical effects by using simplified parameters in a computer model instead of computing them dynamically). By testing the angular momentum conservation equation we can see if the data assimilation phase has actually been consistent with the principles of the conservation of angular momentum or not. For a climate models the data assimilation process does not exist, and here we can learn information about the model's physics.

While testing the observation set or climate model for conservation of Angular Momentum, one has to note that if a reanalysis dataset or climate model conserves angular

momentum it does not mean that it is realistic and giving accurate values of the atmospheric variables. A reanalysis dataset or climate model may be physically internally consistent and conserve angular momentum but not actually be realistic: for example, it may consistently under or over estimates the sizes of events, or for how long they last and when they occur. This noted, physical consistency is still something we want to hope for for good models.

Angular Momentum conservation with previous reanalysis datasets has generally not been achieved, with differences in the angular momentum conservation equation traditionally being quite large. The angular momentum of the earth's atmosphere is linked to the angular momentum of the solid earth through what are known as 'torques', which are forces applied to a body that is rotating about a pivot. The three torques that affect the earth's angular momentum are the mountain torque, the pressure torque and the gravity wave torque. The mountain torque is a torque applied because of the effect of pressure systems on mountains, the friction torque is to do with boundary layer turbulence and friction of the moving wind over the surface, and the gravity wave torque is a torque that resolves subgrid scale processes on the numerical model. The gravity wave torque must be parameterized, yet there is little observed support for the current parametrizatons, Egger et al. (2007). The gravity wave torque is traditionally a strong contributor to this lack of angular momentum conservation, Egger et al. (2007), and we note that interestingly the effect of gravity wave torque has not been studied in the NOAA Twentieth Century Reanalysis Version 2 Reanalysis Observation Dataset (Gil Compo, personal communication).

By investigating and comparing pre-1900 data of the observation dataset, when spatial resolution of an observation dataset was very poor, with results from the late 20th century we also choose to investigate an aspect of our reanalysis observation dataset's gravity wave torque, aswell as the other torques', dependence on the spatial resolution of the *observational network*. Obviously, the number of points recording data and the quality of data has vastly improved over the past 100 years. The reanalysis process interpolates the values over all these years onto the same numerical grid, and therefore by testing the difference in the reanalysis observation dataset's torques over different times, we can detect any dependence of the torques on the observational network's resolution. Note therefore, of course, we are not talking about the resolution of the grid on which the variables are given, but on the coarsity of the observational network used to produce values at each grid point in our reanalysis dataset.

By comparing results of the climate models with that of the reanalysis observation dataset we look at the physical realism of the climate models and extract useful information about their circulation. Also by looking at differences in the climate models over the same time intervals that we look at in the reanalysis observation dataset (for resolution purposes)

we can also look in passing for evidence of model 'drift' (drift is stated in the American Meteorological Society's Online Glossary as "The tendency for the solution of a numerical model integration to move away from its initial conditions and toward its own climate" and is caused by model errors in parameterizations or model imbalances).

We first lay the framework for the project by discussing the angular momentum and torque theory, deriving the equation for conservation of the atmosphere's angular momentum, and explaining the torques that change the atmosphere's angular momentum. We then discuss the angular momentum and torques in relation to the weather patterns, and regional transfer and transport of angular momentum and we further introduce the idea that the atmosphere's angular momentum is linked with the length of day on the earth.

We then discuss the results from previous and similar studies of the angular momentum budget, before we move on to our own computation, and discuss the results of the angular momentum and torques computed on the reanalysis dataset (in relation to angular momentum conservation), and the results from the spatial contribution of the torques in the reanalysis dataset and the climate models.

In the conclusions we then summarise the results and propose further work to do with results from the models that need improvement, such as the torques in the reanalysis datatset and climate models, testing the conservation of angular momentum for the three climate models whose torques we have looked at and testing the conservation of angular momentum on climate models that we have not looked at, and we finalise with an ambitious project on the conservation of angular momentum and gravity wave torque parametrization in the new raised model height Hadley centre climate models.

Chapter 2

Angular Momentum and Torque Theory

2.1 Angular Momentum

Before we consider Angular Momentum of the Earth's Atmosphere we shall consider *linear* momentum. The Linear Momentum, $\mathbf{p}$, of an object is given by

$$\mathbf{p} = m\mathbf{v} \tag{2.1}$$

where m is the mass of the object and $\mathbf{v}$ is the velocity vector. The Angular Momentum of an object (also a vector quantity), and defined as $\mathbf{m}$, may be thought of as the rotational analogue of Linear Momentum. The angular momentum of an object, mass m, is the cross product of the distance $\mathbf{r}$ from an origin $\mathbf{0}$, about which the body rotates, with the mass multiplied by its velocity $\mathbf{v}$, i.e.

$$\mathbf{m} = \mathbf{r} \times m\mathbf{v} \tag{2.2}$$

The force, $\mathbf{F}$, applied to a body is a vector, defined as the mass multiplied by the acceleration, $\mathbf{a}$, of an object, i.e.

$$\mathbf{F} = m\mathbf{a} \tag{2.3}$$

Differentiating (2.2) we get

$$\frac{d\mathbf{m}}{dt} = \mathbf{r} \times \mathbf{F} \tag{2.4}$$

therefore we may see that the rate of change of Angular Momentum of a body is equal to the cross product of its distance from the origin about which it rotates and the total

force applied to the body. This cross product $\mathbf{r} \times \mathbf{F}$ is called the 'Total Torque' applied to the body.

2.2 Torque

A Torque, defined as $\mathbf{T}$, is given by

$$\mathbf{T} = \mathbf{r} \times \mathbf{F} \tag{2.5}$$

If a torque, or a 'turning force', is applied to a rotating object it will slow down or speed up the object's rate of rotation about the origin, or even change its direction of rotation. Through friction and pressure the atmosphere applies these rotational forces to the solid Earth which cause the rotation rate of the solid earth to either speed up or slow down, and in doing so the atmosphere's angular momentum decreases or increases as it imparts or receives angular momentum to or from the earth, thus torques represent the flux of angular momentum across the surface of the earth.

2.3 Mass and Relative Components of Angular Momentum

When we consider the Angular Momentum of the Earth's Atmosphere, we must consider the fact that even if the atmosphere were to stay stationary above the ground, thus not appearing to move, due to the rotation of the Earth the atmosphere would, of course, still be moving. Thus the 'absolute' velocity, $\mathbf{u}_{\text{abs}}$ of an air parcel in the atmosphere, i.e. the velocity relative to a stationary observer who is *not* on the Earth but watching it rotate from afar outside the rotating frame of reference, is the velocity due to the rotation of the Earth added to the relative velocity, $\mathbf{u}_{\text{rel}}$, which is the velocity the air mass has relative to an observer who *is* standing on the Earth. Thus

$$\mathbf{u_{abs}} = \mathbf{u_{rel}} + \Omega \times \mathbf{r} \tag{2.6}$$

where $\Omega \times \mathbf{r}$ is the velocity due to the rotation of the Earth (Ω is the rotation rate of the Earth and $\mathbf{r}$ is the distance of the mass to the point about which the earth rotates).

Recalling (2.2) we see thus that the Angular Momentum of an air parcel of unit mass, defined $\mathbf{L}$, in the Earth's Atmosphere is

$$\mathbf{L} = \mathbf{r} \times (\mathbf{u}_{\text{rel}} + \Omega \times \mathbf{r}) \tag{2.7}$$

and the Angular Momentum of an air parcel of unit volume, $\mathbf{m}$, is

$$\mathbf{m} = \rho \mathbf{r} \times (\mathbf{u}_{\text{rel}} + \Omega \times \mathbf{r}) \tag{2.8}$$

where ρ is the density of the air parcel. Therefore the total Angular Momentum of the Earth's Atmosphere, again a vector, is

$$\mathbf{M} = \int_v \rho \mathbf{L} dV = \int_v \int_v \rho \mathbf{r} \times (\mathbf{u}_{\text{rel}} + \Omega \times \mathbf{r}) dV \tag{2.9}$$

where v is the volume of the atmosphere.

One can also split the Earth's Angular Momentum $\mathbf{M}$, aswell as the velocity, into two conceptually useful parts: the 'mass' part of angular momentum, $\mathbf{M}_\Omega$, and the 'relative' part $\mathbf{M}_\text{r}$. The mass part of the Earth's Angular Momentum is the amount of angular momentum the atmosphere would have if all the atmosphere were at rest vertically and horizontally, staying stationary relative to the ground. The relative part of Angular Momentum is the part of Atmosphere's Angular Momentum that is due to motion of the atmosphere relative to that of the Earth's rotation. Mainly the changes in $\mathbf{M}_\Omega$ are due to changes in the amount of atmospheric mass that there is in a region of the atmosphere, whilst changes in the Relative component are due to wind and any movement.

The mass part is also called the matter term, the pressure term, the Ω term, or the Earth angular momentum term, the relative term is also referred to as the wind term or the motion term, as discussed in Egger et al. (2007).

2.4 The Coordinate System

Due to the rotation of the Earth it is most appropriate to consider variables in a rotating coordinate system. Whilst it is possible to use Cartesian Coordinates to analyse Angular Momentum, throughout this dissertation we adopt the same coordinate system as given by Egger et al. (2007). This means that the Angular Momentum is chosen in the rotating coordinate system shown in figure 2.1, whilst the velocity vector is chosen in the spherical rotating coordinate system. With these choices we write Angular Momentumm as

$$\mathbf{M} = M_1 \mathbf{i}_1 + M_2 \mathbf{i}_2 + M_3 \mathbf{i}_3 \tag{2.10}$$

where i_1 and i_2 lie in the plane of constant latitude 0, where i_1 points, from the centre of the Earth to the Greenwich Meridian, and i_2 points 90° East, and, further, i_3 points outwards from the centre of the earth in a direction parallel to the rotation vector Ω. The rotation vector, which is associated with the rate of rotation, is shown in figure 2.1.

The relationship between the spherical unit vectors $\mathbf{e}_\lambda$, $\mathbf{e}_\theta$, $\mathbf{e}_r$ and the unit vectors in which we express angular momentum $\mathbf{i_1}$, $\mathbf{i_2}$ and $\mathbf{i_3}$ is given in the appendix, and also in

Egger et al. (2007).

Therefore velocity can be written as:

$$\mathbf{v} = u\mathbf{e}_\lambda + v\mathbf{e}_\theta + w\mathbf{e}_r \tag{2.11}$$

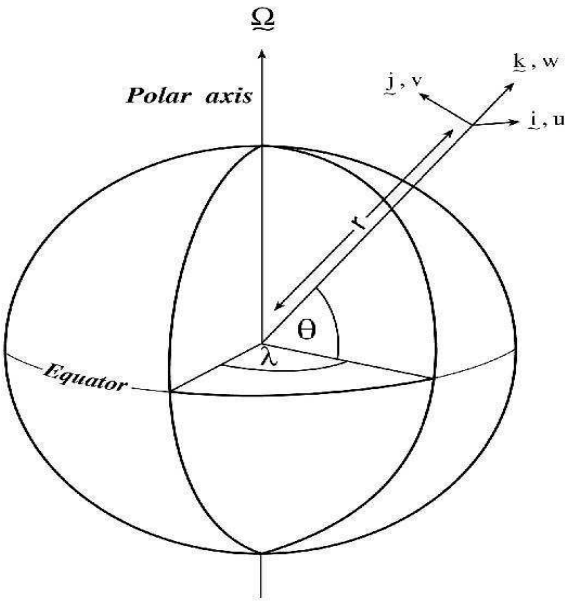

Figure 2.1: Rotating Coordinate System

In this project we will look at the total axial component of atmospheric angular momentum M_3, given by

$$M_3 = \int_V m_3 dV = \int_V \rho(u + \Omega r cos\theta) r cos\theta dV \tag{2.12}$$

which can be seen from equation (2.9), recall the definitions from section 2.3, and note that 'u' is the east-west component of the wind velocity (where a wind moving towards the east is taken as positive, and a wind moving towards the west is taken as negative). We study this component because it is strongly associated with 'east-west' movement across the earth. M_1 and M_2 can also describe the atmosphere, but deal also with the wobble of the earth from it's axis. Note here that this volume v, is bounded by a surface at the outer atmosphere - i.e. where the earth's atmosphere stops - and is bounded by another surface which is the surface of the solid earth (when solid mass is above sea level) and the oceans, when not.

From now on we shall drop the '3' subscript from m_3, M_3, and the Torques, $T_{i,3}$ under the understanding that we will always be refering to the 'third' component of angular momentum and the torque vectors, (thus from now on 'm' should not be taken as or

confused with mass) and similarly, we shall no longer use 'the axial component of angular momentum', but simply 'angular momentum'.

2.5 Conservation of Angular Momentum Derivation

In the following derivation we begin with the time rate of change of angular momentum for a parcel of air and then arrive at the formula for the time rate of change of the angular momentum for the whole atmosphere in terms of two global surface integrals representing the fluxes of angular momentum across the surface of the earth. Note that ρ is the density of parcel, p is the pressure, R is the approximated average radius of the earth and recall λ and θ from figure 2.1 as the angle of longitude and latitude, respectively. Our starting point, as mentioned, is the following formula for the time rate of change of angular momentum of an air parcel, which can be derived from the equations of motion (Peixoto and Oort (2007))

$$\rho\frac{dm}{dt} = -\frac{\partial p}{\partial \lambda} + \rho F_\lambda R cos\theta + \text{tidal and other extraterrestrial torques} \tag{2.13}$$

where F_λ is the Friction Force in the direction of the unit vector e_λ (see appendix 1), the first two terms on the right hand side are torques.

As the tidal and other torques are small we may write the above as

$$\rho\frac{dm}{dt} = -\frac{\partial p}{\partial \lambda} + \rho F_\lambda R cos\theta \tag{2.14}$$

and using

$$\frac{\partial \rho A}{\partial t} = \rho\frac{dA}{dt} - div\rho A\mathbf{u} \tag{2.15}$$

where A is a climatic variable and $\mathbf{u}$ is the velocity vector of an object, it is trivial to see that

$$\frac{\partial(\rho m)}{\partial t} = -div(\rho m\mathbf{u}) - \frac{\partial p}{\partial \lambda} + \rho F_\lambda R cos\theta \tag{2.16}$$

Integrating over the volume v - where v here is defined as the volume bound by the surface s, which is all of the earth's surface inside the two latitudes, ϕ_1 and ϕ_2, with vertical walls at ϕ_1 and ϕ_2, and the imaginary surface at the top of the atmosphere - and employing Gauss's divergence theorem we see

$$\int_v \frac{\partial(\rho m)}{\partial t}dV = -\int_S \rho m u_n ds - \int_v \frac{\partial p}{\partial \lambda}dV + \int_v \rho F_\lambda R cos\theta dV \tag{2.17}$$

where u_n is the normal outward component of $\mathbf{v}$ across the surface S of the volume v. Note, at ϕ_1 this outward normal across the surface points towards the south pole, and at ϕ_2 this outward normal points towards the north pole. The first term on the right hand side corresponds to the flux of angular momentum across these vertical boundaries, whilst the next two terms correspond to the flux of angular momentum across the earth's surface, these fluxes are illustrated in figure 2.2. The physical interpretation of equation (2.18) is that the time rate of change of the angular momentum of the volume v is equal to the transport of angular momentum across its boundaries.

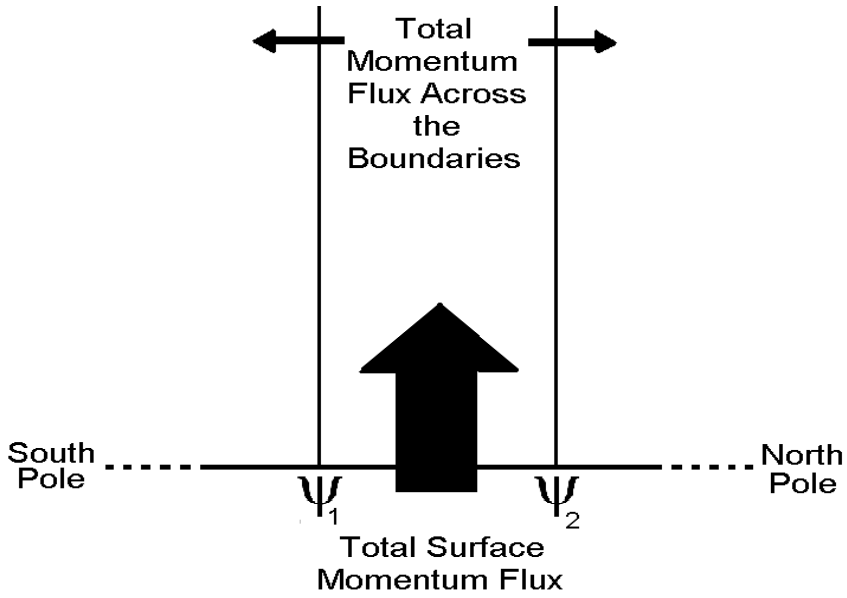

Figure 2.2: Flux of Momentum across the surface of the earth and the vertical atmospheric boundaries enclosing the volume v

We may use the constitutive relation $\mathbf{F} = -\alpha \text{div}\tau$, where $\mathbf{F} = (F_\lambda, F_\theta, F_z)$.

This comes from looking at all the forces acting upon a fluid parcel: if we let δS be a small geometrical surface element with unit normal $\mathbf{n}$ (shown in figure 2.3), and we define τ_{ij} as the j-component of stress on the a surface element δS which has a normal $\mathbf{n}$ pointing in the i-direction, then the zonal (eastward) component of the friction force is

$$F_x = -\frac{1}{\rho}\left(\frac{\partial \tau_{xx}}{\partial x} + \frac{\partial \tau_{yx}}{\partial y} + \frac{\partial \tau_{zx}}{\partial z}\right) \tag{2.18}$$

A more in-depth look on the stress tensor for fluids, and its application to angular momentum may be provided through a combination of Acheson (1990) - who deals mainly with the mathematical treatment of stress tensors for fluid parcels and the Navier-Stokes equations - and Peixoto and Oort (2007) - who deal with the geophysical/meteorological applications.

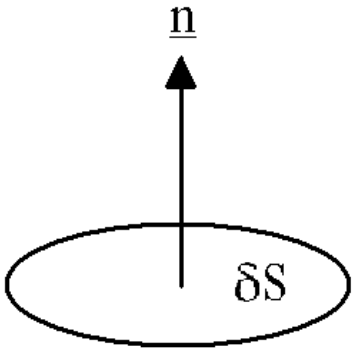

Figure 2.3: Fluid Surface with unit normal **n**

Thus as stated, we use $\mathbf{F} = -\alpha \text{div}\tau$, where $\mathbf{F} = (F_\lambda, F_\theta, F_z)$, and employ Gauss' divergence theorem then

$$\frac{\partial}{\partial t}\int_v \rho m dV = -\int_S \rho m u_n ds - R^3 \int_v \frac{\partial p}{\partial \lambda} dV + \int\int_{sfc} \tau_F cos^2\theta d\lambda d\theta \tag{2.19}$$

where τ_F is the east-west surface stress.

Consider the second term on the right hand side of (2.19), defined Φ,

$$\Phi = -R^2 \int_{\psi_1}^{\psi_2}\int_{sfc}^{\infty}\int_0^{2\pi} \frac{\partial p}{\partial \lambda} d\lambda dz cos\theta d\theta \tag{2.20}$$

(the lower bound of integration 'sfc' stands for the surface of the earth). With a little manipulation this can be changed to be either an integration over pressure levels or a surface integral. For ease of calculation, and also the applicability of particularly relevant literature open to us later on in the project on computation of this term, we choose to take the surface integral.

This means we integrate equation (2.20) by parts, so that we have

$$\Phi = -R^2 \int_{\psi_1}^{\psi_2}\int_0^{2\pi} \left\{ \frac{\partial}{\partial \lambda}\left(\int_{sfc}^{\infty} p dz \right) + p\frac{\partial z_0}{\partial \lambda} \right\} d\lambda cos\theta d\theta \tag{2.21}$$

Noting we may take the partial derivative with respect to λ of $\int_{sfc}^{\infty} p dz$ inside the height integral, and that we may swap the order of integration, we have

$$\Phi = -R^2 \int_{\psi_1}^{\psi_2}\int_{sfc}^{\infty} \left(p(2\pi,\theta) - p(0,\theta)\right) dz d\theta - R^2 \int_{-\pi/2}^{\pi/2}\int_0^{2\pi} p\frac{\partial z_0}{\partial \lambda} d\lambda cos\theta d\theta \tag{2.22}$$

and therefore, as $p(2\pi, \theta) = p(0, \theta)\ \forall\theta \in [-90, 90]$ (because these are the pressure at the same point),

$$\Phi = -R^2 \int_{\psi_1}^{\psi_2} \int_0^{2\pi} \left(p \frac{\partial z_0}{\partial \lambda} \right) d\lambda cos\theta d\theta \tag{2.23}$$

Thus, we note equation (2.19) says the rate of change of angular momentum may be represented by a integral over the vertical surface and two integrals over the earth's surface. If we relabel the last term in (2.19) as Γ and denote the time average of a climatic variable A, over the time interval $[0, \tau]$, as

$$\overline{A} \equiv \frac{1}{\tau} \int_0^{\tau} A dt \tag{2.24}$$

and we take the long time average of equation (2.19), and use (2.23), we see we have

$$0 = -\overline{\int_S \rho m u_n ds} + \overline{\Phi} + \overline{\Gamma} \tag{2.25}$$

therefore

$$\overline{\int_S \rho m u_n ds} = \overline{\Phi} + \overline{\Gamma} \tag{2.26}$$

showing us that over a long period of time, the flux out of the volume of atmosphere, v, across the vertical boundaries, shown in figure 2.2, is equal to the flux into the the volume of atmosphere across the surface of the earth.

If we extend the integrals in equation (2.19) to the cover the whole globe, i.e. $\psi_1 = 90$ $\psi_2 = -90$, then equation (2.19) becomes

$$\frac{dM}{dt} = \Phi + \Gamma \tag{2.27}$$

i.e. we have a formula for the time rate of change of the total global atmospheric angular momentum in terms of two surface integrals. Physically, this formula states that the rate of change of the total Atmospheric angular momentum is equal to the sum of all the torques, i.e. the 'rotating forces', acting on the earth's surface.

The total atmospheric Angular momentum can ONLY be transferred across these surfaces because we see that angular momentum is a conserved quantity. A region in the atmosphere can exchange angular momentum with another region of the atmosphere, but the total atmospheric angular momentum cannot be lost through these exchanges - only through exchanges across the surface of the earth. We note in passing that similar, but slightly more complicated, coupled equations between the 'equatorial' components of angular momentum (M_1 and M_2) exists.

Theoretical understanding is shone on equation (2.27) when we see that Φ is what is

called the mountain torque, which we now define as T_M. This is the torque that occurs due to the pressure exerted on any raised surface (and importantly pressure exerted on mountains), and that Γ is what is called the friction torque, T_F, which is the torque from the friction applied by the atmosphere to the surface of the earth. Thus (2.27) becomes

$$\frac{dM}{dt} = T_M + T_F \tag{2.28}$$

It is important to note, that throughout this project we take, in line with convention, that a torque that increases the angular momentum of the atmosphere to be a positive torque, and one that decreases the angular momentum of the earth to be a negative one.

Although equation (2.28) holds true analytically, when we work on numerical models we need to add another torque. This torque, called the gravity wave torque, is the part of the mountain and friction torque too small to be resolved on a numerical grid, we shall discuss this in more detail in 2.8. Thus for numerical models a form equivalent to (2.28) may be given where, on the right hand side, the gravity wave torque is included, so that we have

$$\frac{dM}{dt} = T_M + T_F + T_G \tag{2.29}$$

Of course this means

$$M(t) - M(0) = \int_0^t T_F + T_M + T_G \; dt \tag{2.30}$$

and it is interesting to note that equation (2.26) implies that over long periods of time the total torque time average over a long period of time is zero i.e. there is no change in the angular momentum of the atmosphere over long periods of time.

We shall now summarise the main torques.

2.6 Friction Torque

The friction torque is the torque that is exerted on the earth's surface due to the frictional force that occurs because of the wind directly above the Earth's surface moving relative to the solid earth. If there is an net global westerly surface wind (i.e. a surface wind *from* the west) the atmosphere will speed the earth's rotation up, transfer angular momentum to the earth, and thus the atmosphere loses angular momentum. Analogously, if there is a net easterly surface wind (i.e. a surface wind *from* the east), the atmosphere slows down the rotation of the earth and angular momentum is transferred from the earth to the atmosphere. The Friction Torque is given by

$$T_F = R^3 \int_{\lambda=0}^{2\pi} \int_{\theta=-\pi/2}^{\pi/2} \tau_f cos^2\theta d\theta d\lambda \tag{2.31}$$

where τ_F is the average east-west surface friction stress per unit area, and R is the average radius of the earth from its centre.

2.7 Mountain Torque

Mountain Torque is a function of pressure and orography and is the 'turning force' exerted due to a difference in pressure across any raised surface on the earth, but most significantly, mountains or mountain massifs. Consider a mountain with a high pressure on the west side of a mountain and low pressure on the east. The pressure system will exert an eastward torque that causes the earth to increase it's rate of rotation, imparting angular momentum from the atmosphere to the solid earth. The opposite case, where there is higher pressure on the east side of the mountain, will slow the earth's rotation down, reducing the solid earth's angular momentum, and imparting it to the atmosphere.

Mountain Torque is given by

$$T_M = -R^3 \int_{\lambda=0}^{2\pi} \int_{\psi=-\pi/2}^{\pi/2} p_{sfc} \frac{\partial h}{\partial x} cos^2 d\psi d\lambda \tag{2.32}$$

and note that this may be written

$$T_M = R^3 \int_{\lambda=0}^{2\pi} \int_{\psi=-\pi/2}^{\pi/2} h \frac{\partial p_{sfc}}{\partial x} cos^2 d\psi d\lambda \tag{2.33}$$

which originates from equation (2.20), as shown by Peixoto and Oort (2007). Indeed on a planet with no mountains or raised surfaces there would not be any mountain torque.

2.8 Gravity Wave Torque

The Gravity Wave Torque is the part of the Mountain and Friction Torque that is too small to be resolved by current Global Circulation Models - the nature of the grid spacing, and particularly the coarse resolution on climate models means a large number of Mountains and Mountain-induced waves are not resolved, as mentioned in Egger et al. (2007) and Palmer et al. (1987). For example, mountains usually have very jagged terrain, and far below the size of the grid used there can be turbulence and pressure applied to the mountain that will not be picked up by the model, thus we introduce the gravity wave torque as a way to remedy this.

Note that we talk about pressure and turbulence over mountains, and in this light, at

this scale, it is quite hard to separate what is the friction torque and what is mountain torque in a model, and this is why we said the gravity wave torque was the part of the mountain and friction torque too small to be resolved.

The gravity wave torque is given by

$$T_G = R^3 \int_{\lambda=0}^{2\pi} \int_{\theta=-\pi/2}^{\pi/2} \tau_g cos^2\theta d\theta d\lambda \tag{2.34}$$

where τ_G is the average east-west surface gravity wave stress per unit area.

2.9 Other Torques

There are numerous Torques that act to change the Angular Momentum of the Atmosphere, however they are a lot smaller than mountain, friction and gravity wave torques, and did not appear in the above derivation because we ruled the corresponding terms at the start of our derivation. A comprehensive discussion of things that can produce torques is given in Weickmann and Sardeshmukh (1994), we very briefly mention a few of these 'other' torques.

There are torques from *outside* the earth-atmosphere-ocean (EAO) system, such as solar winds, electromagnetic forces, and a tidal torque exerted by the moon and other planets on the Earth that causes a slow secular decrease in the angular momentum, this corresponds to a loss rotation of about 2 ms/century, Peixoto and Oort (2007).

There are also a number of other Torques coming from within the EAO system such as the Moisture or Precipitation Torque and the Ocean or Continent Torque. However the contributions from all these torques are negligible in comparison to the mountain, friction and gravity wave torque, as mentioned in Peixoto and Oort (2007) and Egger et al.(2007). For the angular momentum budget of the atmosphere the friction and mountain torques are both essential, and this has long been realised, e.g. White (1949).

Chapter 3

Angular Momentum and Atmospheric Circulation and Variability

Angular momentum is transferred on a large range of timescales, such as daily, interannual, annual and so on because the atmosphere is a dynamical system with large variability and events occuring on all manner of timescales.

The friction from the wind is perhaps the simplest example of angular momentum transfer, and presssure and weather systems exerting a mountain torque on the earth (aswell as a friction torque) is another. These transfers occur on relatively short timescales (days), whilst transfer on interdecadal timescales are due to, for instance, the El-Niño Southern Oscillation (ENSO) - which is a quasi-periodic climate pattern that occurs in the pacific ocean, on average every 5 years - and on annual timescales, associated with the strength of the high altitude west to east fast flowing air currents called the jet streams, and there is also a major source of intraseasonal variation of the atmospheric angular momentum from Tropical Convection, and in particular, the Madden Julian Oscillation (MJO) - which is a pattern of coupling between atmospheric circulation and convection around the Indian Ocean that occurs every 30-60 days. The importance of torques due to the atmospheric circulation and variability on time scales shorter than a season are debated, as mentioned by Weickmann and Sardeshmukh (1994) and Madden and Speth (1995), and Weickmann and Sardeshmukh (1994) discuss, at length, the link between the MJO and angular momentum.

As discussed there is also angular momentum transfer, that is not weather or climate related, on century length timescales which occur because of the effect of tidal friction from the moon and planets, and, as not discussed, on interdecadal timescales to do with the

angular momentum exchanges between the atmosphere and earth involving the processes of the solid earth's inner geological processes shown by Peixoto and Oort (2007).

3.1 Regional Angular Momentum Transfer and Transport

We now know that there is an exchange of Angular Momentum between the Earth and the Atmosphere, and that it is facilitated by pressure differences across mountains and raised surfaces, and the friction between the Earth and the Atmosphere from the relative movements of the air over the surface of the Earth. However, the specific details where this transfer through the torques and then the corresponding transport occurs has not, so far, been discussed, and shedding light on these will be the topic of the next few pages. It should be noted that angular momentum transport and transfer becomes clear when long time averages are considered. Recall over long time intervals the flux across vertical boundaries is equal to the flux across the surfaces, and by taking long term averages we can understand the general flow of angular momentum through the atmosphere.

3.1.1 Friction Torque

Recall that when the wind directly above the surface in a region is a westerly wind, i.e. $u > 0$, there is a friction force applied to the atmosphere from the earth in the opposite direction to the surface wind, (surface stress, which is force per unit area, is $\tau > 0$), and the torque in that region applied to the earth's surface is less than zero, thus increasing the angular momentum of the Earth and decreasing the Angular Momentum of the Atmosphere. For a surface wind, $u < 0$, the force is applied in the opposite direction, and the torque in that region is greater than zero, and the atmosphere increases it's Angular Momentum.

A sketch of the Earth showing a generalised motion of the surface winds is shown in figure 3.1. Note generally around the equator the motion of the surface winds is from the East to the West, thus we expect to see in observations that the friction torque is greater than zero in this latitude band, and the movement in the midlatitudes (the region approximately $30° - 60°$ North or South of the equator) is approximately from the West to the East, and so we expect to see the friction torque being less than zero in observations of these regions.

We see this pattern in figure 3.2, where the latitudinal torque profile - a plot of the averaged torque over all longitudes (called the zonal average) for each circle of constant latitude - has been calculated at each latitude by Madden and Speth in their investigation. I.e.

$$\frac{1}{2\pi}\int_0^{2\pi} A(\lambda,\theta)d\lambda \tag{3.1}$$

is plotted($\forall\theta$). Note the whole term in (3.1) is commonly defined as [A(θ)]. In agreement with our general wind pattern discussed above we see that, on average the Friction Torque is positive in areas where the average wind direction is West to East, and negative where the average wind direction is West to East. In weather and climate studies Torques are generally given in the unit Hadleys or 'Had', where 1 Had = 10^{18}kg m^{2}s^{-2}. The values in the graph, a discretized form of (3.1), are given not $\forall\theta$ but for latitude strips, which is why we see the units are Hadleys per degree.

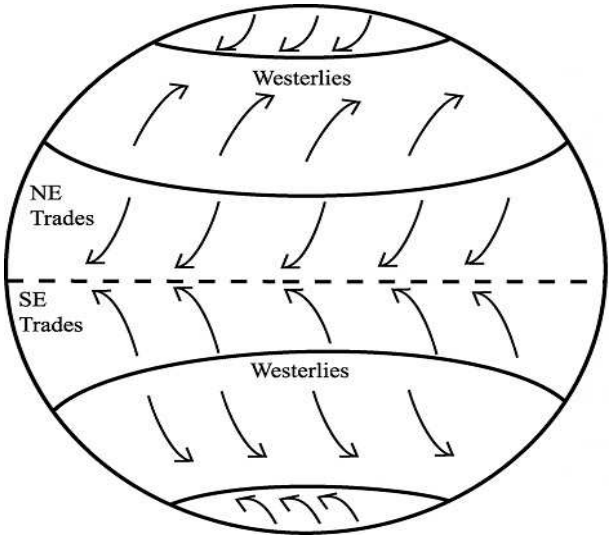

Figure 3.1: Prevailing Surface Winds

3.1.2 Mountain Torque

The Himalayas and the Rocky Mountains have been shown to be big contrubutors to mountain torque activity as mentioned in Weickmann et al. (2007). At the Himalayas and the Rocky Mountains generally Angular Momentum is lost and the atmosphere is decelerated due to the (time averaged) pressure differences across these mountain ranges. The Andes also plays a role, albeit a smaller one, as mentioned in Oort (1989), Weickmann and Sardeshmukh (1994), and Madden and Speth (1995). Figure 3.3, shows, in agreement, the mountain torque latitudinal profile.

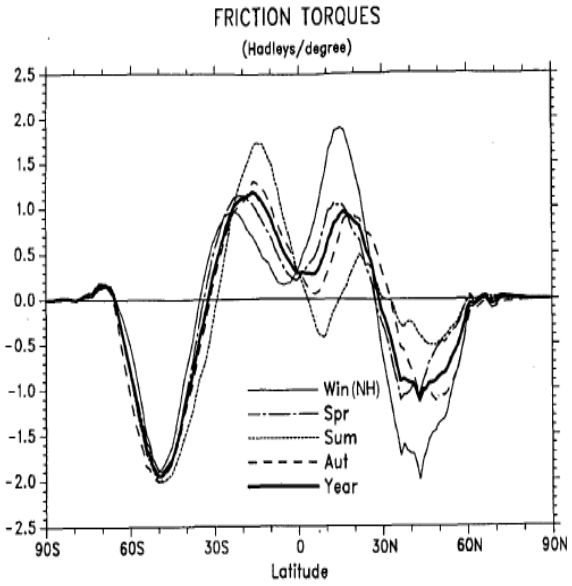

Figure 3.2: Friction Torque Latitudinal Profile. A zonal average of T_F over June 1987-May 1988, from Madden and Speth (1995).

3.1.3 Gravity Wave Torque

We could not find a latitudinal profile for the gravity wave torque, however there is little doubt that the magnitude of the gravity wave torque, simply because it is the unresolved part of the mountain and friction torque, will be large around the the major mountain ranges i.e. the rocky mountains and the himalayas.

3.1.4 Angular Momentum Transport

We are now able to draw a rough picture: Angular Momentum enters the Atmosphere through Friction Torque around the Equator and then the Friction Torque at the midlatitudes and the Mountain Torque and mainly the Himalayas and Rocky Mountain Ranges sap the atmosphere's angular momentum.

Because Angular Momentum is sent into the the Earth at midlatitudes (a sink for the atmosphere) and a source for the atmosphere is the 'excess' angular momentum that comes out of the Earth at the equator there must be a flow of angular momentum from the equator to the midlatitudes through the atmosphere and a flow from the midlatitudes to the equator in the oceans or the solid Earth.

Poleward movement of angular momentum occurs through either the movement of mass in the atmosphere or midlatitude waves or Eddies. The significance of the midlatitude waves or eddies to the poleward contribution of angular momentum was shown by Victor

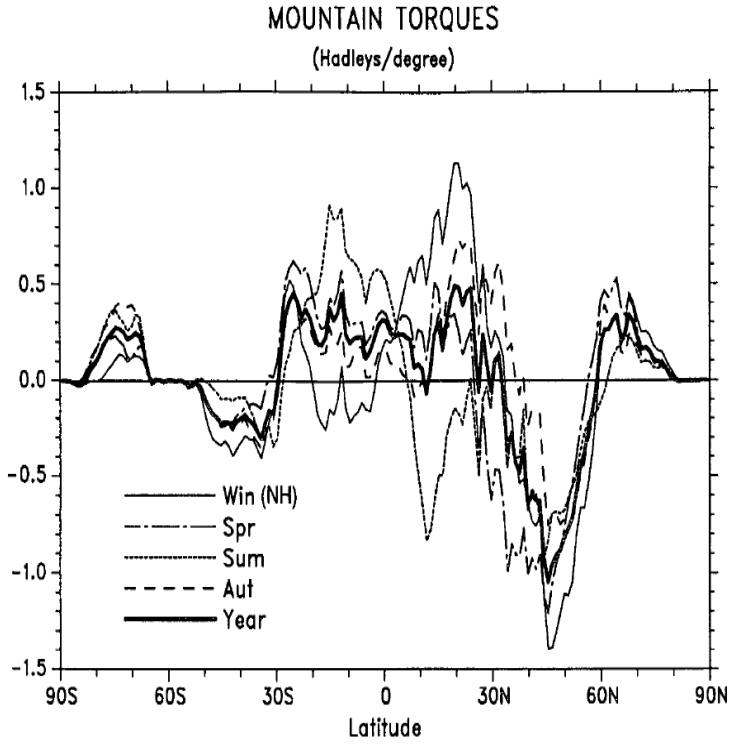

Figure 3.3: Mountain Torque Latitudinal Profile. A zonal average of T_M over June 1987-May 1988, from Madden and Speth (1995).

Starr, as mentioned in Oort (1989).

The right hand side of figure 3.4 shows the streamlines of angular momentum through the atmosphere, where ψ_M is the flux of angular momentum (the left side does not show angular momentum transport, but shows the average wind speeds in the atmosphere).

Angular momentum streamlines are a set of curves instantaneously tanget to the velocity of the flow of angular momentum through the atmosphere. As discussed, as there is a flux of angular momentum into the earth at the midlatitudes, angular momentum must then be transported back to equatorial regions (roughly the region within the latitudes 23°N-23°S).

The oceans were postulated to tranport angular momentum back down into the equatorial regions, but as shown in Peixoto and Oort (2007) oceanic transports are about 100 times too weak to be able to transport all the angular momentum required back to the equatorial regions. As is detailed in Peixoto and Oort (2007) and Egger et al. (2007), it is suggested that where angular momentum is transferred into the oceans at the midlatitudes the oceans transport simply transfer the angular momentum back to the Solid Earth and then all excess angular momentum at the midlatitudes travels back through the Earth. One suggested process is a "prefered tilting" of the motions along the faults in the conti-

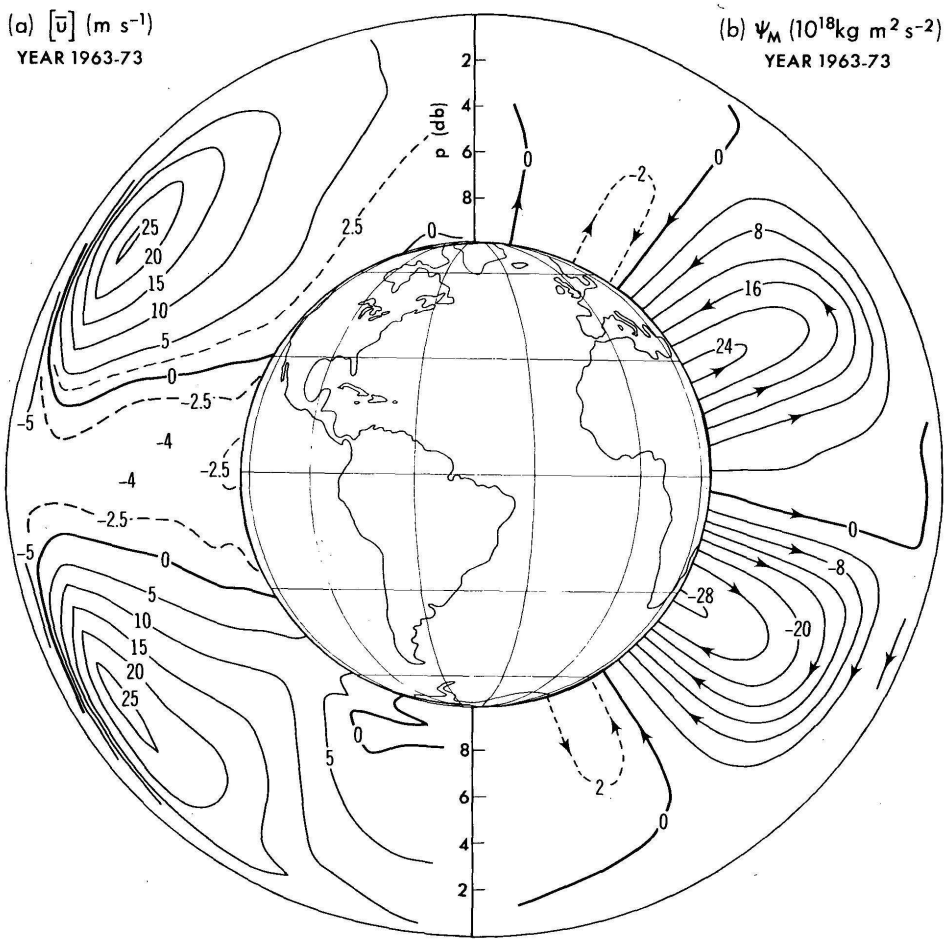

FIG. 11. Cross sections of (a) the mean zonal flow in the atmosphere in units of m s^{-1}, and (b) the streamlines of relative angular momentum in Hadley units, both for annual mean conditions 1963–73 (after Oort and Peixóto 1983). Note that the vertical scale of the atmosphere is grossly exaggerated.

Figure 3.4: Cross sections of the mean zonal flow in ms^{-1} on the left hand side of the earth in diagram (a), and the streamlines of the relative angular momentum in (b). Note that the diagram is not to scale and the size of the atmosphere is greatly increased. Diagram originally from Oort (1989)

nents, Oort (1989), i.e. there is a possibility that angular momentum is transferred back through the earth by earthquakes! This would have to occur on long timescales. On short timescales the solid earth would accumulate these torques and then release them in bursts through the Earthquakes. Despite that this is uncertain, the implications of it being true are very large, and if true, the torques would link the motions within the Atmosphere and Oceans, to motions in the Earth's Crust. Indeed this link has been, and is being, pursued further e.g. Zharov (1996), but further discussion on this area shall not be given here.

3.2 Changes in the Length of Day and Atmospheric Angular Momentum

The angular momentum of the atmosphere increases and decreases in an annual cycle due to the seasons. The angular momentum of the atmosphere is at its largest in the northern hemisphere winter, and is at its minimum in the northern hemisphere summer due to, in part, what is described in Egger et al. (2007) as a northern hemisphere "variability excess" over the summer hemisphere.

Recall that the jet streams are high altitude fast flowing air currents. The jet northern hemisphere jet streams reaches its highest speeds in the northern winter and its lowest speeds in the northern summer, and the southern hemisphere jet stream reaches its highest speeds in the northern summer and its lowest speeds in the northern winter, however, as shown in Peixoto and Oort (2007), its summer maximum is not as large as the northern hemisphere jet's winter maximum.

As discussed, because the total amount of angular momentum of all of the earth, oceans and atmosphere is constant, when the angular momentum of the atmosphere is increases the angular momentum of the earth decreases, and vice versa, and as we have seen there is an annual cycle of angular momentum, we can see that there is an annual cycle of the angular momentum of the solid earth.

When the angular momentum of the atmosphere is at its minimum, the angular momentum of the solid earth is at its maximum, and when the angular momentum of the atmosphere of the atmosphere is at its maximum the angular momentum of the earth is at its minimum.

This annual cycle in the angular momentum of the atmosphere and thus the earth actually means that the rotation rate, and therefore length of day (LOD), of the earth changes in accordance: times of high atmospheric angular momentum correspond to a longer than average length of day and times of lower atmospheric angular momentum correspond to a shorter than average length of day.

A graph showing measurements of the Angular Momentum of the Atmosphere and the LOD is given in figure 3.5.

We can gain a simple, approximate, formula for the change in the length of day by observing the following derivation. The conservation of angular momentum means that the total angular momentum of the solid earth and the atmosphere is constant. Thus

$$I_{\mathrm{e}}\Omega + M_{\mathrm{rel}}\mathrm{constant} \tag{3.2}$$

i.e.

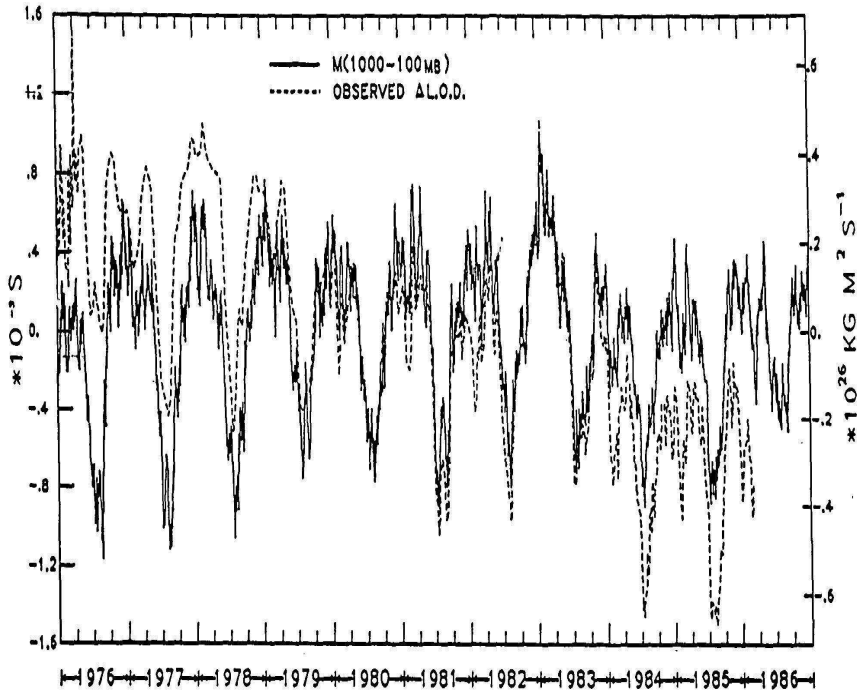

Figure 3.5: LOD and Relative Angular Momentum, from Peixoto and Oort (2007)

$$I_e\Omega + \int_{V_{atm}} \rho urcos\theta dV = \text{constant} \tag{3.3}$$

where Ω is the rate of rotation of the solid earth, i.e. $\Omega = \frac{2\pi}{T}$ where T is the period of one rotation, I_e is the moment of inertia of both the solid earth and atmosphere (i.e. if it were stationary above the solid Earth). Therefore

$$\Delta(I_e\Omega) + \Delta M_\text{Rel} = 0 \tag{3.4}$$

Thus

$$\Delta\Omega = \frac{\Delta M_\text{Rel}}{I_\text{e}} \tag{3.5}$$

and because

$$\Delta\Omega = -\frac{2\pi\Delta T}{T^2} = -\frac{\Omega\Delta T}{T} \tag{3.6}$$

we see

$$\frac{\Omega \Delta T}{T} = -\frac{\Delta M_{\text{Rel}}}{I_{\text{e}}} \tag{3.7}$$

Defining $\Delta T = \Delta LOD$, and using $I_{\text{e}} \approx 7.04 \times 10^{37}\text{kg m}^2$ the change in the length of day then can be given (see Rosen et al. 1987) by the following formula:

$$\Delta LOD = 0.168 \Delta M_{\text{Rel}} \tag{3.8}$$

where ΔLOD is in units of milliseconds (ms) and ΔM_{Rel} is in units of $10^{25}\text{kg m}^2\text{s}^{-1}$. This yields approximately a 0.8 ms increase in the LOD at July than the LOD in January and this corresponds to a $2ms^{-1}$ change in zonal wind.

There have been debates about the value for the momentum of inertia of the solid earth in this calculation. The solid earth is composed of many different layers, but may be grouped into three main layers, and from inside to outside they are: the core, the mantle and the crust. Debates are present as to whether the mantle and crust may be rotating at a different rate to the liquid core, and as noted by Peixoto and Oort (2007) this is the reason for why the moment of inertia was chosen as $7.04 \times 10^{37}\text{kg m}^2$ instead of other suggested values which perhaps ignore the rate of rotation of the liquid core (which has been suggested to be different to that of the mantle and crust of the earth).

The angular momentum of the atmosphere and oceans is *very* small compared to that of the Earth. The angular momentum of the atmosphere is roughly $1.02 \times 10^{28}\text{kg m}^2\text{s}^{-1}$ (The average value of the relative angular momentum of the atmosphere is about $1.3 \times 10^{26}\text{kg m}^2\text{s}^{-1}$ whilst the mass component of angular momentum is $1.01 \times 10^{28}\text{kg m}^2\text{s}^{-1}$), the oceans (and snow) have generally been regarded to be unimportant to the changes in angular momentum. The total angular momentum of the solid earth is roughly $5.86 \times 10^{33}\text{kg m}^2\text{s}^{-1}$, as shown in Peixoto and Oort (2007), thus we see that the atmospheric angular momentum is of five orders smaller than the solid earth's angular momentum. To recap: we see that the length of day of the earth changes due to angular momentum transfer into and out of the earth, occuring primarily in the regions previously discussed. However, one shocking idea is that, despite the size of the solid earth, the atmosphere appears to be speeding up and slowing down the earth, rather than the earth controlling the atmosphere, a discussion of this is given in Oort (1989). Indeed in Oort (1989) it is mentioned that "it seems that the tail of the elephant is driving the elephant around!".

It is interesting to note in passing that there have been a few spectacular and rapid changes in the angular momentum of the Earth. One example is that of May 20 1979 to June 1 1979 where the zonal wind speed dropped by $1.5ms^{-1}$ and the LOD decreased by about $0.6ms$ as mentioned in Peixoto and Oort (2007).

Chapter 4

Angular Momentum Budget studies in the Literature

We now discuss the results obtained in previous research papers, and whilst getting ideas on how to test the datasets, we also find information about what we should see.

Angular Momentum conservation with reanalysis datasets has generally not been achieved. Differences in the angular momentum tendency and total torques have traditionally been of the order ±10 Had, with gravity wave torque a strong contributor to this imbalance, Egger (2007). Some previous angular momentum budget studies just concern themselves with the mountain and friction torque from the outset, e.g. Madden and Speth (1995). Huang et al. (1999) suggested that the gravity wave torque was overestimated in NCEP-NCAR reanalysis data.

Egger et al. (2007) calculate the angular momentum and torques from National Centers for Environmental Prediction (NCEP) over the period 1958-1997. They include a figure, shown here as figure 4.1, that displays the seasonal cycle of friction torque, gravity wave torque and mountain torque, aswell as the angular momentum, the tendency of angular momentum and the sum of the torques. One should pay careful attention to the different scales that are used for the angular momentum and the torques in diagram (a). The units the torques are expressed in are Had and are shown on the left hand vertical axis, the units the angular momentum is expressed in is 10^6Had s and is displayed on the right hand vertical axis, in (b) all plots use the same axis shown on the left hand vertical axis.

The graph shows again a discrepancy of 10 Hadleys between the total torque and angular momentum tendency and that the gravity wave torque addition causes a large negative total torque with what is a roughly constant bias of 10 Had between the angular momentum and total torque, however, the inclusion of the gravity wave torque significantly improves the shape of the total torque curve.

The power spectrum of the angular momentum calculated by Egger et al. (2007) is

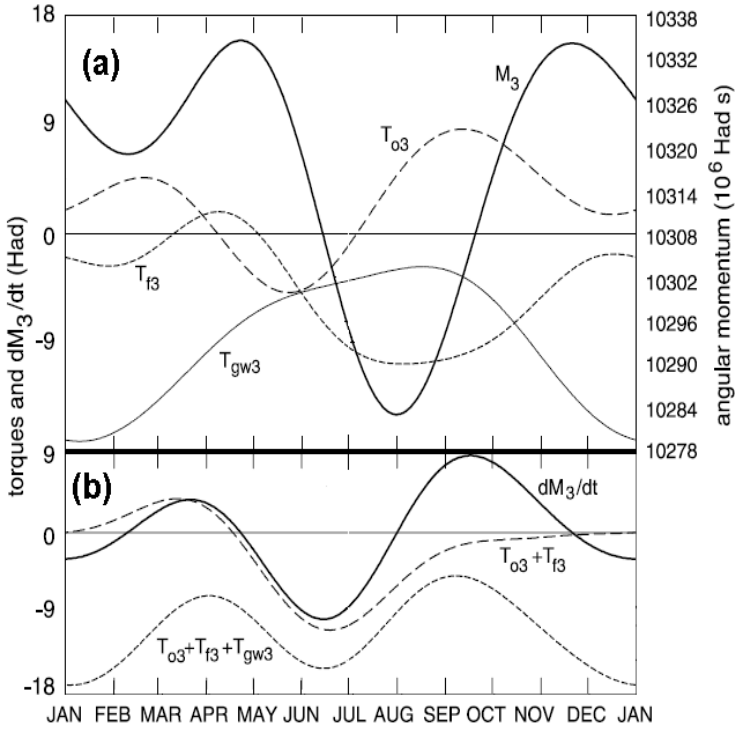

Figure 4.1: (a) All Torques and Angular Momentum - note the different scales (b) Angular Momentum tendency and summation of the torques. Figure adapted from Egger et al. (2007)

shown in figure 4.2. The power spectrum is the energy per unit time of a signal for a (user specified) range of frequencies. It allows us to see processes occuring on a given timescale. To provide an example, consider the Quasi Biennial Oscillation (QBO) - the QBO is a cycle of the equatorial zonal wind in the tropical latitudes in the stratosphere; the winds switch from easterlies to westerlies and back to easterlies, and so on, in a quasi-periodic fashion on average 28 to 29 months (roughly in the region of 850-880 days). Indeed, such a cycle does show up in the angular momentum signal of Egger et al. (2007): around just under 1000 days there is a large peak in the power spectrum due to a combination of the QBO and ENSO showing influence of the QBO and ENSO on angular momentum, whilst the broad peak at higher frequency is due to seasonal and intraseasonal variability.

Madden and Speth (1995) look at angular momentum and mountain and friction torques over a 13 month period during 1987 and 1988. They see that conservation of angular momentum with their data, from the European Centre for Medium Range Weather Forecasts (ECMWF), is poor. They first look at the integrated version of the torques (i.e. equation (2.30)) and it can be seen that their integrated total torque does not match up at all well with the angular momentum calculated from the model, see figure 4.3, and

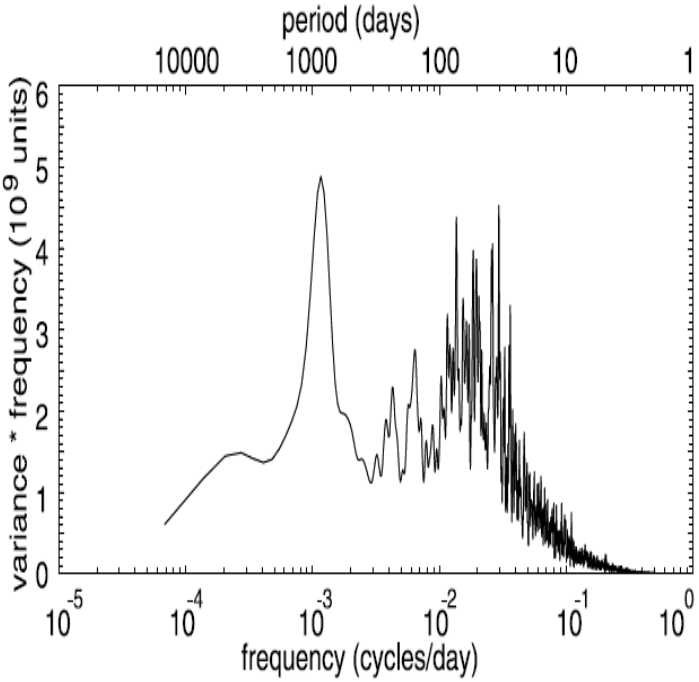

Figure 4.2: A power spectrum of the angular momentum from Egger et al. (2007). The data is from the National Centers for Environmental Prediction (NCEP) over 1958-1997.

they suspect that their error in their balance comes from friction torque. They calculated the value of friction torque using friction stress from a forecast model (that calculated estimates of the friction stress from the raw data), rather than using just the raw data for friction stress, because this was expected to give better estimates due to a more sophisticated formulation for the friction torque and vertical atmospheric stability information from the forecast model. However, their values of friction torque, given by the forecasts had a serious negative bias, which leads to a spurious result for the value of the total torque integration. Their lack of conservation may be preserved significantly better if they add a value of 12.1 Hadleys to their to the value of the torques. They conclude that they strongly suspect some of the answer may reside in bias in the friction torque from the forecast model, though further work would be required to be sure of this. Again (as with Egger et al. (2007)) we see that the total torque tends to be negatively biased. However, despite their poor lack of conservation of angular momentum Madden and Speth (1995) note the torques do show many of the subseasonal changes that occur in the angular momentum.

The idea we raised in the introduction, that a model could be physically internally realistic although poorly out of sync with reality, has been tested before by, e.g. Egger et

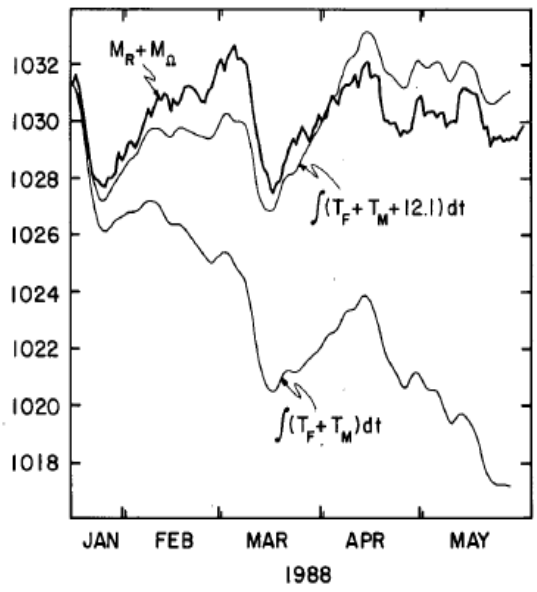

Figure 4.3: Angular Momentum and the Integrated Total Torque over Jan-May 1988, with and without an addition of 12.1 Had to the Total Torque, from Madden and Speth (1995). Units are 10^{25}kg m^{2}s^{-1}, i.e. 10^7Had.

al. (2003), who make intercomparisons of the NCEP and ECMWF reanalysis datasets.

In their paper Egger and Hoinka (2002) look at the links between the torques and found that the mountain and friction torques appeared to act on the Atmospheric Angular Momentum as if the torques were independent of each other, however they are not. An example of this can be seen in Weickmann (2003), where wave trains (a succession of similar waves in the atmosphere) around the pacific ocean and the west of North America were shown to contribute to the Mountain Torque and provide a dynamical link between the mountain torque activity and friction torque activity off the west coast of North America. Weickmann (2003) found wave trains shift high sea level pressure systems over east asian and north american mountain ranges, and cause a negative mountan torque whilst these wavetrains can also cause a positive friction torque that then counteracts the effects of the negative mountain torque on the atmospheric angular momentum.

Moreover, there have been many experiments producing slightly differing results with regards to the torques and their contributions. Weickmann et al. (1997) point out how Weickmann and Sardeshmukh (1994) found in their investigation that the mountiain and friction torques contribute about equally to changes in atmospheric angular momentum, however that Madden and Speth (1995) found the mountain torque to be much larger contributor to changes in the atmospheric angular momentum.

As pointed out in Weickmann et al. (1997), Rosen (1993) shows the contribution of

mountain and friction torque to the total torque depends on the timescale. Weickmann et al. (1997), further point to Swinbank (1985) who showed on synoptic scales that the mountain torque is much larger than the friction torque, and Madden and Speth (1995) who showed that this dominance continues out to at least 20-day fluctuations. However, within the timescale of interest to Weickmann et al. (1997), the two contribute about equally to the global torque, while in the zonal budget the friction torque is larger.

Chapter 5

Datasets

In this project we look at a reanalysis dataset and 3 climate models. We take data climate model data from the World Climate Research Programme's (WCRP's) Coupled Model Intercomparison Project phase 3 (CMIP3) multi-model dataset, described an "unprecedented collection of recent model output". The WCRP CMIP3 Multi-Model Database serves the serve IPCC's Working Group 1 (who focuses on the physical climate system - the atmosphere, land surface, ocean and sea ice). Information on the comprehensive specifications of the models is given at:
$http://www-pcmdi.llnl.gov/ipcc/model\_documentation/ipcc\_model\_documentation.php$

5.1 Model Specifications

The NOAA Twentieth Century Reanalysis Version 2 Observation Dataset is produced by the Earth System Research Laboratory Physical Sciences Division from the NOAA and the University of Colorado CIRES/Climate Diagnostics Centre. It is on a regular grid (constantly spaced grid points) of 2 degree spacing in latitude and 2 degree spacing in longitude for surface pressure and surface height. Friction stress, gravity wave stress, are u wind velocity are given as monthly mean values calculated from 8-times Daily 3-hr Forecasts forecast model on a Gaussian Grid with 192×94 grid points (roughly 2.0 degree latitude (changing separation in latitude because it is a Gaussian Grid) by 1.75 degree longitude). There are 23 pressure layers in the vertical from 1000hPa to 10hPa, inclusive. Further information is given at
$http://www.esrl.noaa.gov/psd/people/gilbert.p.compo/20CRv2\_Compoetal2010.pdf$.

The HadCM3 climate model is produced by the UK Met Office's Hadley Centre. It is a on regular grid of 2.75 degrees spacing in latitude by 3.75 degrees spacing in longitude for surface pressure, surface height and surface friction stress. We do not calculate an-

gular momentum on the climate models so need not concern ourselves with their vertical layers, and the gravity wave stress is not given in any of the models in the WCRP CMIP3 multi-model database. Full information on the model is given at
$http://www-pcmdi.llnl.gov/ipcc/model\_documentation/HadCM3.pdf$

The HadGEM1 climate model is produced by the UK Met Office's Hadley Centre. It is on a regular grid of 1.25 degrees spacing in latitude by 1.875 degrees spacing in longitude for surface pressure, surface height and surface friction stress. Full information on the model is given at
$http://www-pcmdi.llnl.gov/ipcc/model\_documentation/HadGEM1.pdf$,

The NOAA GFDL CM2.0 climate model . It is on a regular grid of 2 degrees spacing in latitude and 2.5 degrees spacing in longitude for surface pressure, surface height and surface friction stress. Full information on the model is given at
$http://www-pcmdi.llnl.gov/ipcc/model\_documentation/GFDL-cm2.pdf$

5.2 Access

Authorised access to the NOAA Reanalysis observation dataset is not required and data can be downloaded directly from their website
http://www.esrl.noaa.gov/psd/data/gridded/data.20thC_ReanV2.monolevel.mm.html However, access must be granted to the WCRP CMIP3 Multi-Model Dataset before one can begin to download the data from the website $https://esg.llnl.gov:8443/$

Chapter 6

Computation

6.1 How we compute

Many of the discrepancies in the angular momentum budget are very large and our choice of calculation does not require heavily compex schemes because we are not studying minute variations, however, in particular the mountain torque due to its derivative term requires special attention. We list here, only how we have chosen to calculate - a discussion of the considerations needed to be taken into account and the different ways to calculate these terms is given in Appendix 1.

6.2 Angular Momentum

Angular momentum can be written as

$$M = M_\Omega + M_r = \frac{R^4\Omega}{g}\int_{10}^{1000}\int_{\lambda=0}^{2\pi}\int_{\theta=-\pi/2}^{\pi/2} p_{sfc}cos^3\theta d\theta d\lambda + \frac{R^3}{g}\int_{10}^{1000}\int_{\lambda=0}^{2\pi}\int_{\theta=-\pi/2}^{\pi/2} ucos^2\theta d\theta d\lambda dp \tag{6.1}$$

as seen in Madden and Speth (1995). The limit 10hPa of the pressure integral is due to the fact that this is the roof limit for our, and many other, models. Ideally we would like to integrate over the whole of the atmosphere, however this is a reasonable approximation.

We take the approximation

$$M \approx \frac{R^4\Omega}{g}\sum_i\sum_j p^{i,j}_{sfc}cos^3\theta_j\Delta\theta_j\Delta\lambda_i + \frac{R^3}{g}\sum_i\sum_j\sum_k u_{i,j,k}cos^2\theta_j\Delta\lambda_i\Delta\theta_j\Delta p_k \tag{6.2}$$

where for variable A $A_{i,j,k}$ means the value of A at point (i,j,k). $A^{i,j,k}$ is also defined as this, and is used for when an existing subscript is already present for name of the variable

itself.

It is important to be aware of potential potholes when working with velocities given on pressure levels. Consider a hill on which the surface pressure at three grid points lying on a line of constant latitiude is 990hPa, 987hPa, and 981hPa.

Velocity in the datasets is given on pressure levels of 1000hPa, 950 hPa, 900hPa, and so on (though not necessarily always decreasing by 50 hPa). If we were to try to integrate over the full volume of the atmosphere (1000hPa to 10 hPa) because the pressure at the surface at the three points is 990hPa, 987hPa, and 981hPa, between 990hPa and 1000hPa, or 987hPa and 1000hPa, or 981hPa and 1000hPa, there is no atmosphere! So we must make sure to set values of velocity, corresponding to the velocity on the 1000hPa level, in our code, to zero when integrating the u-velocity over this region.

However, we will now have moving air between 987-950hPa (say) that is not accounted for, therefore we integrate the relative momentum over 950hPa and weight this volume integral by the difference of the 950hPa level and the surface pressure, i.e. we multiply by (987-900)/(950-900).

Also, consider what would happen if the surface pressure were not 987hPa, but 1017hPa, then we would need to weight the volume integral, corresponding to the velocity given at 1000hPa, for that interval by (1017-950)/(1000-950). This only applies to the *first* volume box that is directly above the surface, and integrating over the rest of the atmosphere we do not need to consider weighting.

This consideration applies not only for the 1000hPa level, but for all the surface terrain, including where there is a mountain that could cause the surface pressure of e.g. 587hPa.

6.3 Friction Torque

For the friction torque in the reanalysis dataset, as with the climate models, the value of friction stress is explicitly given, therefore we do not use calculate the stress by parameterization of the surface drag coefficient (this is a quantity used in the formulation of the friction stress which corresponds to how much resistance something will encounter when moving over a surface, a high/low drag coefficient means large/small resistance). This parameterization of the drag coefficient has been done in the past e.g. Wahr and Oort (1984). We calculate friction torque by

$$R^3 \int_0^{2\pi} \int_{-\pi/2}^{\pi/2} \tau_F cos^2\theta d\theta d\lambda \approx R^3 \sum_i^N \sum_j^M \tau_F cos^2 \Delta\theta_j \Delta\theta_i \tag{6.3}$$

In the reanalysis dataset the friction stress is given from a model forecast, and in that sense our approach is similar to that of Madden and Speth (1995). In the climate models

the friction stress is simply the value of friction stress directly from the model itself, and not from a forecast model that has processed the direct output.

6.4 Mountain Torque

For mountain torque we take

$$T_M = R^2 \int_{-\pi/2}^{\pi/2} Y_M cos\theta d\theta \approx R^2 \sum_{j}^{M} Y_{M,j} cos\theta_j \Delta\theta_j \tag{6.4}$$

where

$$Y_M = -\int_0^{2\pi} p \frac{\partial h}{\partial \lambda} d\lambda \approx \sum_{i}^{N} p_i \sum_{k=-K}^{k=K} b_k h_{i+k} = \sum_{i}^{N} \sum_{k=-K}^{k=K} p_i b_k h_{i+k} \tag{6.5}$$

and where we take the sixth ordered centered difference scheme as given by Weickmann and Huang (2008), shown in the table below

Table 6.1: 6th Order Centered Scheme b_k coefficients

k	-3	-2	-1	0	1	2	3
b_k	-1/60	3/20	-3/4	0	3/4	-3/20	1/60

On the NOAA Reanalysis datset the mountain torque was calculated by the pressure given by the dataset.

6.5 Gravity Wave Torque

We take the approximation

$$T_G = R^3 \int_{\lambda=0}^{2\pi} \int_{\theta=-\pi/2}^{\pi/2} \tau_G cos^2\theta d\theta d\lambda \approx R^3 \sum_{i}^{N} \sum_{j}^{M} \tau_G cos^2 \Delta\theta_j \Delta\theta_i \tag{6.6}$$

for gravity wave torque. With the gravity wave stress τ_G taken from the forecast model.

6.6 Conservation Equations

We approximate the angular momentum tendency by

$$\left(\frac{dM}{dt}\right)_n \approx \frac{M_{n+1} - M_{n-1}}{2\Delta t_n} \tag{6.7}$$

6.7 netCDF Files

The files containing the data come in the form of 'netCDF' ('.nc'),which are the common form of storage file for Observation Datasets and Climate Models, and can be opened directly with MATLAB provided the version being used is 7.7 or later (which all have built in support for reading and writing netCDF files).

The values in the Climate Models do not need to be changed from the values in the files.

The values in the NOAA observation set for a variable, however, are not actually the true values of that, but are 'packed' values, in an effort to reduce the size of the files. To get the true value one must perform a simple 'unpacking' using two constants, specific to that .nc file. First one must multiply by a constant or 'scale factor' (which may be equal to one), and to add another constant, or 'offset' (which may be equal to zero). For example, consider one wished to extrapolate value of u wind velocity at March 1871 at latitude 0, and longitude 0 on pressure level 850hPa, then we would need to call the value that is given in the file, and then multiply the value by the scale factor and add the offset. We are required to input the pressure level, latitude, longitude, and time. The netCDF file also contains information about the other variables (such as the pressure levels on which u is calculated), so we need to also have a 'variable identifier', which is just a number. For the appropriate file we input argument in the form

"netcdf.getVar(Filename, Variable Identifier, [(Latitude Position on Grid) (Longitude Position On Grid) (Pressure Level) (Month))"

Consider the command "netcdf.getVar(UWIND,5, [0 45 3 2])". This instructs MATLAB to retrieve information on a variable from the netCDF file i.e. "netcdf.getVar" from the netCDF file labelled as "UWIND" ('u'-wind means the east-west wind). The next number, 5, corresponds to the fifth variable of the file (the u-wind), and the following set of numbers in the '[ ]' parentheses correspond to 0 degrees latitude (the 0th value of latitude as the first grid point is at 0 degrees), 0 degrees longitude (the 45th longitude value, as the file starts at 90 degrees north longitude and goes down to -90 degrees south), on the 850 hPa pressure level (the fourth pressure level - 1000hPa, 950hPa, 900hPa, 850hPa), and March 1871 (the '2' for the third month - 0 means January 1871, 1 means February 1871).

And retrieving the scale factor and offset with
"netcdf.getAtt(UWIND,5,'scale_factor'))", i.e. the scale factor to be multiplied to the 5th variable, and "netcdf.getAtt(UWIND,5,'add_offset')", i.e. the offset to be added to the 5th variable. Then the true value for the monthly average u wind at 0 degrees latitude 0 degrees longitude, at 850hPa over March 1871, which we call u_{true}, is given by

$$\text{Unpacked Value} = \text{Offset} + (\text{Packed Value} \times \text{Scale Factor}) \tag{6.8}$$

where

- Offset=netcdf.getAtt(Zero,5,'add_offset')
- Packed Value=netcdf.getVar(Zero, 5, [0 45 3 2])
- Scale Factor=netcdf.getAtt(Zero,5,'scale_factor')
- Unpacked Value = u_{true}

Thus one gains the true value of the u wind variable from the .nc file.

6.8 Latitudinal Profiles

For the latitudinal profile of the climatic variable A, we take the approximation

$$\frac{1}{2\pi}\int_0^{2\pi} A(\lambda,\theta)d\lambda \approx \frac{1}{2\pi}\sum_i A(\lambda_i,\theta_j)\Delta\theta_j \tag{6.9}$$

for j=1,...,N where N is the number of grid points and where $\Delta\theta_j$ is a width or a 'latitudinal strip', dependent on the spacing in the grid.

6.9 What we compute

To compute angular momentum is to compute over a 3D field, whilst to compute torques is to compute over a 2D field. In fact with 23 pressure levels, despite we require a weighting system for the velocity on the pressure levels which increases computational expense, it is a good approximation to say that angular momentum is 23 times more computationally expensive than the torques. Whilst we would like to have a full angular momentum investigation for all four models it is beyond the scope of the project because of available computational power.

Indeed most angular momentum budget studies look at the angular momentum of one, perhaps two, datasets, sometimes over a year, sometimes over 30 or 40 years. We constrain ourselves to a 30 year investigation of the reanalysis datasets angular momentum and torques, and we further compute and compare the average monthly torque latitudinal profiles from all the datasets over two decades 1890-1899, and 1990-1999, however for the climate models we have only the mountain and friction torque because, as mentioned before, the gravity wave stress is not explicitly given in any of the climate models in the WCRP CMIP3 multi-model dataset. The latitudinal profiles allow us to see if we not

only have the correct total value of torque, but if the torque is coming from the right regions, and allows us to investigate the relative importance of certain mountain ranges, for example. To compare the torques of a climate model with the torques of an observation dataset we must take averages, say decadal averages (rather than looking at individual torque values of the climate model) to see if they represent the processes well *statistically* as climate models cannot hope to predict specific events, but the overall statistical state of the atmosphere.

If we test the angular momentum over the period 1961-1990, it will be a period of time that is long enough to confirm if angular momentum conservation occurs, aswell as a period with accurate observational recordings and it is also a time period on which other models have been tested, so gives us the opportunity to use, and compare and contrast with other experiments, which is especially important, given the rarity of testing in this area on this dataset.

Chapter 7

Results

The results from the NOAA Reanalysis Observation Dataset and the Climate Models show many commonalities with previous investigations whilst also having some interesting differences. However, the differences, which naturally occur between datasets, should not hold us back from saying that the agreement between our results calculated here and other papers over specific details gives us confidence that our results are correct. Such examples of this (which we shall discuss) are the range of values seen from our calculations and the range of values seen in previous investigations, the yearly average time series of angular momentum and the latitudinal friction profiles.

There are three points to take into account for reading the graphs

1. Sometimes we write 'AM' instead of Angular Momentum on the axes of the graphs when writing Angular Momentum would be too large to fit on the graph or would clutter the axes.

2. We also take the average yearly time series (as done in Egger et al. (2007), shown here as figure 4.1). The x-axis ranges from 1-12, where 1 is January and 12 December.

3. Lastly, in the latitudinal profiles that we plot a negative value of latitude corresponds to the degrees south of the equator, whilst a positive latitude corresponds to degrees north of the equator.

We first consider the time averages of the angular momentum and all the torques on the reanalysis dataset, then the latitudinal profiles of all the torques in the reanalysis, and then we consider the latitudinal profiles of all the torques in the climate models.

7.1 The NOAA Reanalysis Dataset

7.1.1 Time Averages from the NOAA Reanalysis Dataset

We can see in the annual average plot of angular momentum that the annual maximums and minimums of angular momentum occur in the winter and summer, repectively, as they should do. We can clearly see that the angular momentum shows very close agreement in shape, and the basic underlying physics, with Egger et al. (2007). The angular momentum is larger than seen in other papers however, e.g. Madden and Speth (1995), and assuming superrotation (which is the idea that a planet's atmosphere rotates separately from, and faster than, the solid planet itself, and is taken here as a very crude approximation so that we can derive an approximate average speed of the whole atmosphere relative to the surface), the atmosphere has an a fairly small average velocity u_0, of $u_0 \sim 5\text{ms}^{-1}$ over 1961-1990, compared to Egger et al. (2007) that have $u_0 \sim 7\text{ms}^{-1}$, because of a smaller relative angular momentum in the NOAA reanalysis observation dataset (and thus the mass part of the angular momentum is quite large).

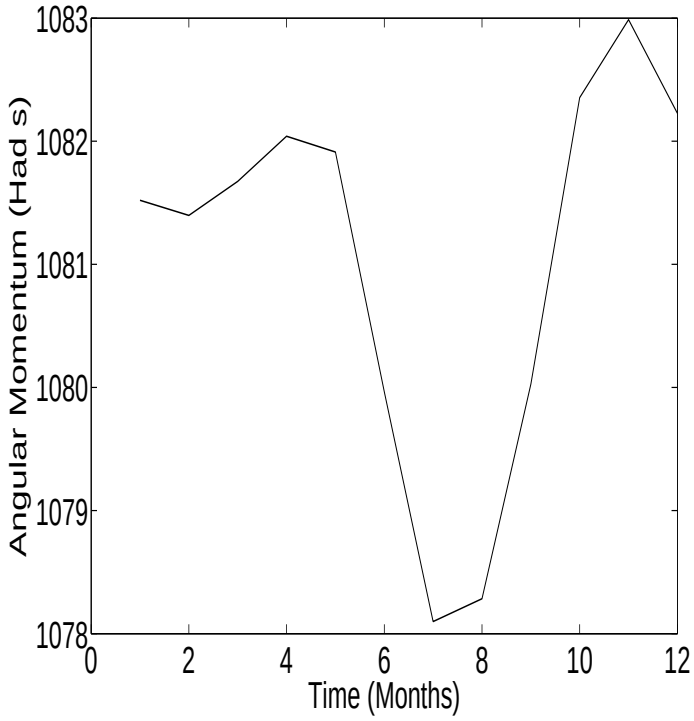

Figure 7.1: Year Average of the Reanalysis Dataset's Angular Momentum over 1961-1990

The 30 year average mountain torque shows many features that we would expect, and shows general agreement with Egger et al. (2007). We note that the minimum in the

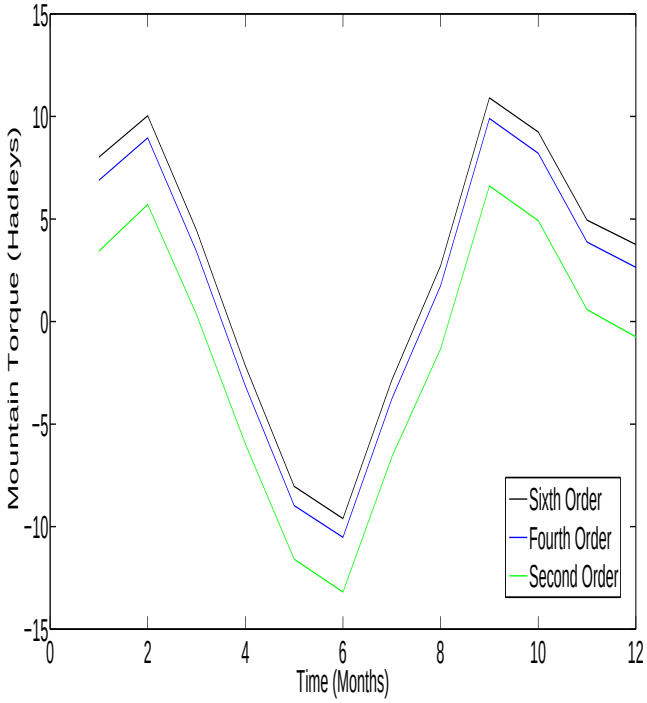

Figure 7.2: Year Average of the Reanalysis Dataset's Mountain Torque using three different centered schemes over 1961-1990

reanalysis observation dataset is about twice the size as that of Egger et al. (2007), and the reanalysis has a larger february peak than Egger et al. (2007). This means that at the time of minimum mountain torque we can expect more high pressure systems on the west side of the most important mountain ranges (contributing a steep negative gradient to the angular momentum tendency). The average value of the mountain torque over 1961-1990 is 2.8 Had - compare Huang et al. (1997) with 2.5 Had, and Egger et al. (2007) with -5 to -3 Had, indeed as noticed by Egger et al. (2007) the time mean value of mountain torque is highly uncertain. We calculated the mountain torque with three finite difference schemes, discussed in great detail in appendix 2, and we can see that, in line with previous research on the effect of the schemes conducted by Weickmann and Huang (2008), the lower the order scheme used, the more negative the value of mountain torque. Indeed, we see here a lower order causes a negative shift over all values of the mountain torque by a constant. The fact that the fourth order mountain torque is considerably closer to the sixth order scheme shows the rapid convergence to the true solution as the order used is increased that Weickmann and Huang (2008) speak of (indeed the difference between the sixth order scheme and higher order schemes would be negligible). Indeed, for the total torque investigations we took the most accurate value of mountain torque (sixth order).

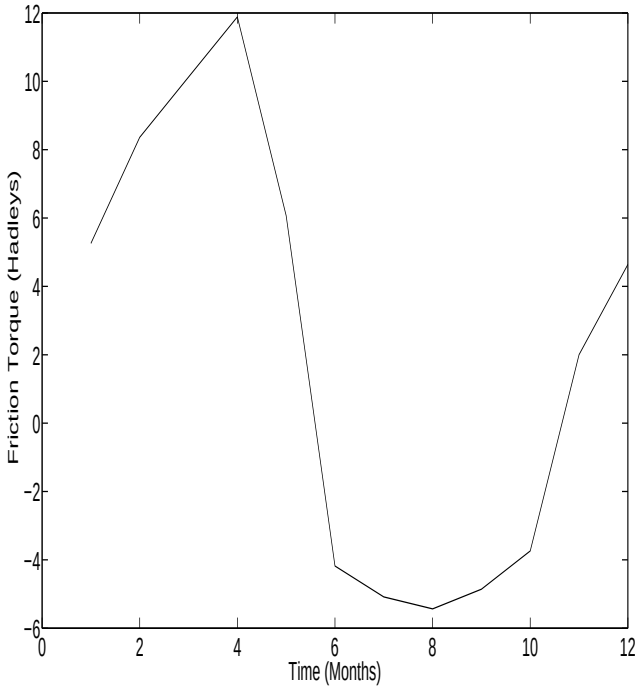

Figure 7.3: Year Average of the Reanalysis Dataset's Friction Torque over 1961-1990

Again the 30 year Friction Torque average shows us the same general properties in terms of shape as Egger et al. (2007), with the timings of minimums and maximums again in agreement, implying larger contribution from easterly surface winds than westerly surface winds across the whole globe in the northern hemisphere spring, and the reverse in the northern hemisphere autumn. We note however that the torques appear to be shifted up by a few Hadleys at over all months in comparison to Egger et al. (2007), especially in the northern hemisphere winter and spring - the time at which the mountain torque is larger than that of Egger et al. (2007) aswell. The average value of friction torque in the reanalysis is 2 Had, and for Egger et al. (2007) it is roughly -6 Had, whilst Madden and Speth (1995) found a staggering -18 Had from their angular momentum budget studies - and as we have seen they discuss the idea that they have a very large negative bias in the friction torque. The value of 2 Had is larger than normal, which tends to be around -6 Had, as mentioned in Egger et al. (2007).

The values of gravity wave torque suggest it is too important to ignore it in our angular momentum conservation study, and the values we see are of the same range as seen in Egger et al. (2007), i.e. from roughly -3 Had (in July) to roughly -15 Had (in March). The average value of the gravity wave torque over 1961-1990 is -8.8 Had (compare Egger

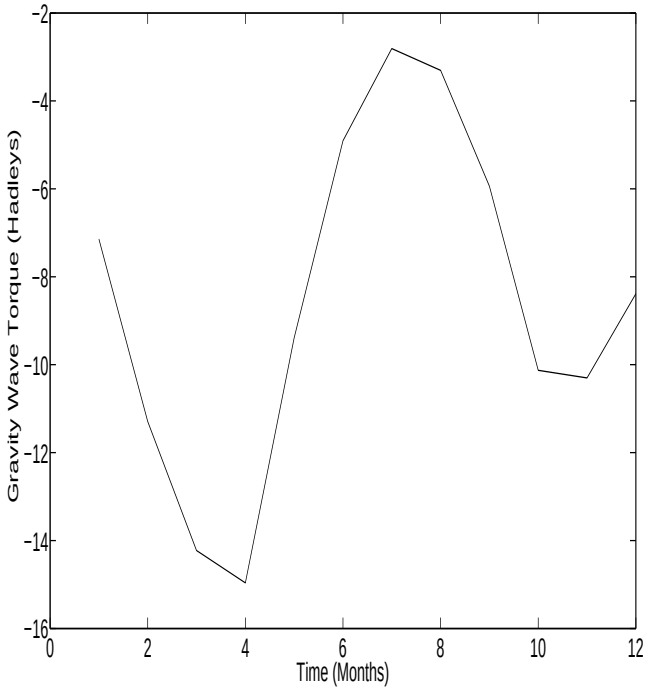

Figure 7.4: Year Average of the Reanalysis Dataset's Gravity Wave Torque

et al. (2007) who had -7.6 Had). The gravity wave torque graph, however, is significantly different to that of Egger et al. (2007). It has a very large winter rise, whilst in Egger et al. (2007) the gravity wave torque actually decreases during the winter months.

There is a rise in the gravity wave torque when the mountain torque is at its most active in removing angular momentum from the atmosphere, and the gravity wave torque appears like a mirror image of the mountain torque but delayed by one month so that when mountain torque increases/decreases the gravity wave torque decreases/increases.

We noticed another possible physical link with the gravity wave torque and the mountain torque. Whilst attempting to understand why the NOAA reanalysis gravity wave torque is as it is, it was also found that the seasonal cycle of gravity wave torque has the same shape as mountain torque, but that the gravity wave torque is two months *ahead* of the mountain torque. Shifting the gravity wave torque by two months so that the gravity wave torque at january is moved to be at march, and the value at february is moved to be at april, march to may and so on the graphs rise and fall together, and suggests a possible link through a lag time. The shifted two month shifted gravity wave torque plotted with the mountain torque can be seen in figure 7.5, however the physical cause for this, if it is a true link, remains unclear. Indeed, recalling that the gravity wave torque is the unresolved

part of the mountain torque it would be peculiar for the gravity wave torque to precede the mountain torque in such a fashion.

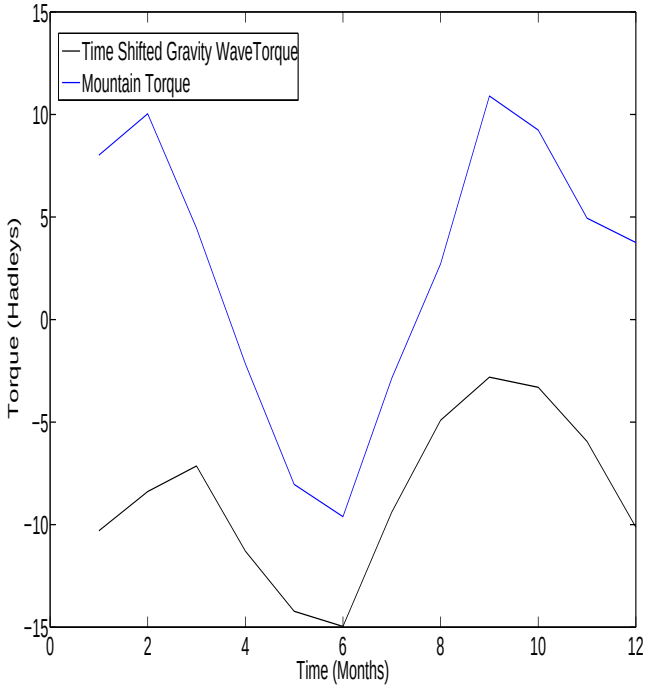

Figure 7.5: Time Shifted Year Average Gravity Wave Torque with 30 Year Average Mountain Torque

Figure 7.6 is the 30 year average of angular momentum tendency and total torque. These values of the angular momentum tendency and total torques belong to the same range of values as has been seen in Egger et al. (2007), and Madden and Speth (1995). Specifically, the angular momentum tendency shows good agreement in terms of the shape of the graph, with Egger et al. (2007) and Madden and Speth (1995) (their angular momentum tendency not shown) - as we would expect since our 30 year average of angular momentum showed good agreement.

Accordingly we see that the angular momentum tendency is at its lowest in june, a month before the minimum angular momentum is reached, and at its highest in september, two months before the highest value of angular momentum.

The total torque, however, is different to Egger et al. (2007), and whilst it appears in Egger et al. (2007) that their total torque is different to the angular momentum approximately by a constant value, the NOAA reanalysis observation dataset has a more complex disparity between the tendency and the total torque. The average total torque is less than the average angular momentum tendency from march through to, and inclusive

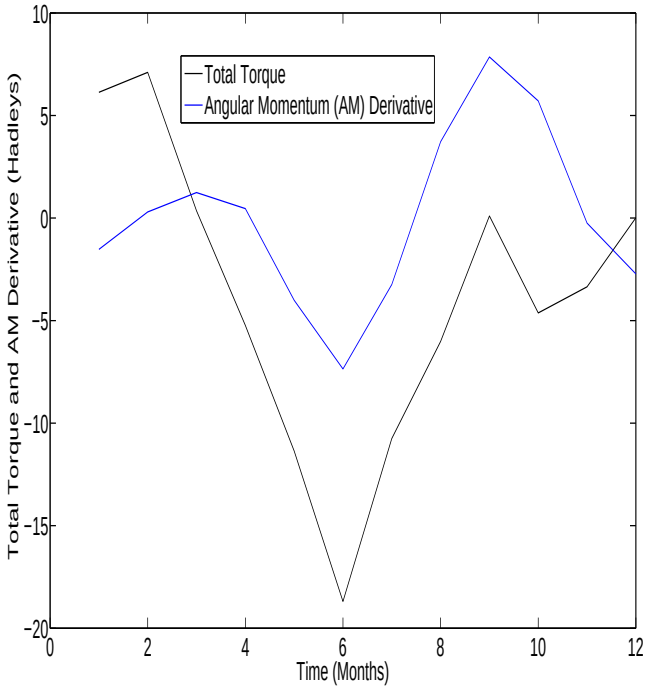

Figure 7.6: Yearly Average of the Reanalysis Dataset's Angular Momentum Tendency and the Yearly Average Total Torque over 1961-1990

of, november, with the difference between the two typically in the range of 5 and 10 Hadleys. Whilst the total torque shows the june-july minimum and a peak in september as with Egger et al. (2007), it does not, in the winter months, resemble at all what can be seen in Egger et al. (2007). Of course results taken from Egger et al. (2007) should not be treated as absolute truth, but the comparison between these results with the results of another research project is very useful to us, and we look at reasons as to why we do not have a similar shape.

An inspection of the individual torque averages shows that such a pattern during the months where our total torque does not agree with that of Egger et al. (2007) - of a large january to march drop and an increase from september to october and moreso from november to december - can be seen in the gravity wave torque's average.

The gravity wave torque from the reanalysis observation dataset shows, rather than a winter decrease of the values from september onwards as is seen in Egger et al. (2007), an increase, with january's gravity wave torque 8 Had more than april's. Without this winter increase, we see that the difference between what we have and a gravity wave torque like that of Egger et al. (2007) in the winter would be the right size to ameliorate the unexpected shape of the total torque to that of just a total torque that is different

to angular momentum tendency by roughly an addition by a constant. However, despite this problem, the average total torque is -3.8 Had $(-8.8 + 2.8 + 2.2)$ (the closer to zero the better due to the requirement of total torque being zero over long periods of time as discussed in section 2.5), and indeed the fact that sometimes the total torque exceeds the angular momentum tendency suggests that here there is a better yearly balance between the torques and angular momentum tendency than in Madden and Speth (1995), where torque is always less than the angular momentum, requiring an addition of 12.1 Hadleys to balance the torque with the angular momentum.

Mindful that the gravity wave torque appears to have large error in it in the winter, although in the summer it agrees fairly well with Egger et al. (2007), we removed the gravity wave torque completely and plotted the yearly average of the mountain and friction torque added together against the angular momentum tendency to see if there would be better agreement.

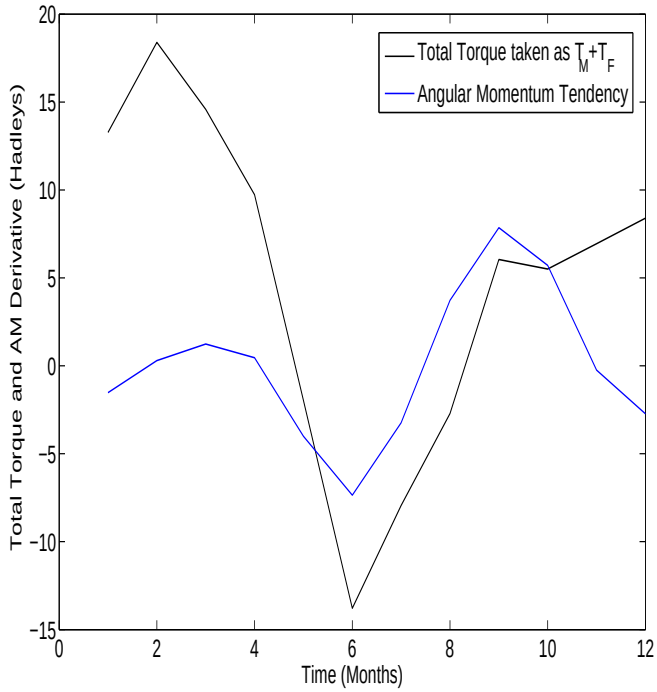

Figure 7.7: Yearly Average Angular Momentum Tendency and Yearly Average Total Torque, with the Total Torque taken as the sum of Mountain and Friction Torque

With just the total torque taken as the mountain torque added to the friction torque it can be seen that we get a northern hemisphere february local maximum, a june local minimum, and a septmeber local maximum, which we also have for the angular momentum tendency (except the first local maximum is in march, not february) demonstrating the

seasonal cycle, and that during the northern hemisphere summer months there is much stronger agreement.

However, there is a very large difference between the total torque and the angular momentum tendency values in the northern hemisphere winter/spring, and a large peak is still existent - we recall mentioning the very large values of mountain and friction torque in the northern hemisphere winter compared to Egger et al. (2007) - and it appears that there is a perhaps some error associated with the northern hemisphere winter/spring period, considering also that the gravity wave torque failed to look similar to Egger et al. (2007) through this period aswell.

The fact that all torques exhibit large anomalies in the northern winter suggest that it would not be just the gravity wave torque parametrization causing the gravity wave torque error, although there may be error in the parameterization, and error in all the torques implies error in the data assimilation process used to create the torques in the NOAA reanalysis dataset.

Graphs of the timeseries for the angular momentum and torques were discarded, as they showed little more than the oscillatory behaviour displayed in the annual averages giving little information and they were deemed not complimentary to the discussion.

There is, however, one extra piece of information we took from them, that the averages could not display, before we discarded them. This was whether the angular momentum or the torques over time were seen to be decreasing, constant, or increasing. Lines of best fit were plotted, and this helped us extract useful information on this. It was easily seen that the line of best fit for angular momentum indicated a small increase over 1961-1990, this increase however was only an increase of $\sim 1/1000$ of the value of angular momentum, and was not considered a significant increase, especially over thirty years. Thus it appears that angular momentum is fairly good at abiding to the theory which says that the angular momentum of the atmosphere, over long time scales, must remain constant.

The lines of best fit for the torques showed a large decrease. The line of best fit for the mountain torque displayed a decrease of 5 Hadleys whilst for the friction torque we saw a line of best fit that decreased by 6 Hadleys, whilst we saw a 1 Hadley decrease for the gravity wave torque over the 30 years. As the torques range between -15 Had to 15 Had the decrease in the mountain and friction torque, especially, are considered significant.

This decrease of the torques over 1961-1990 suggests the mountain and friction torques clearly seem to have some underlying error. One, or two, of the torques may decrease over a significantly long time but the total torque should not decrease or increase because of the idea discussed before that says the angular momentum should not increase or decrease over long periods of time (over long periods of time no increase or decrease in the angular momentum implies that the total torque should not change as $\frac{dM}{dt} = T_M + T_F + T_G$), however here we see a slight increase in the angular momentum, and yet a decrease in all

the torques. Therefore we see conflict between what is happening, and what should be happening. Even if the dataset were to have decreasing torques and to have a *decreasing* angular momentum, we would see that whilst decreasing over long periods of time, which it should not do, it could still be *internally* consistent. Here we see a clear indication that the angular momentum and the torques in the NOAA reanalysis dataset are physically disjoint.

We reason that perhaps some of the disparity between the angular momentum tendency and the total torque is due to this constant decrease in the torques, and we decided to take a yearly average of the first fifteen years to compare it with a yearly average of the last fifteen years over 1961-1990. Taking the average yearly average angular momentum tendency and total torque for the first fifteen years one can see that, with the exception of the erroneous months of january to march and december, there is a much closer agreement between the total torque and the angular momentum tendency than when we look at the last fifteen years, and it is believed that, along with the torques' peculiar winter peak not seen in Egger et al. (2007), the decrease in the mountain and friction torques over thirty years contribute a good deal to explaining the difference between the angular momentum and the total torque. The yearly average over 1961-1975 and the yearly average over 1986-1990 are shown in figures 7.8 and 7.9, respectively.

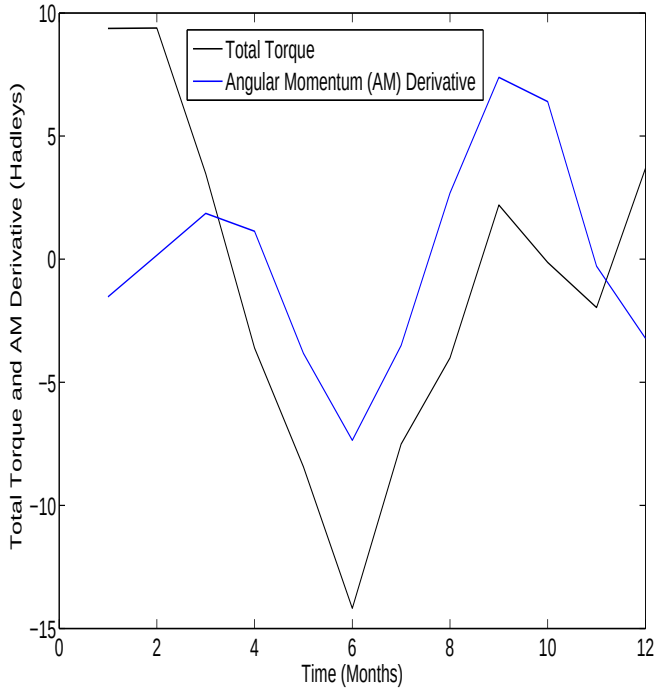

Figure 7.8: Yearly Average Angular Momentum Tendency and Total Torque for 1961-1975

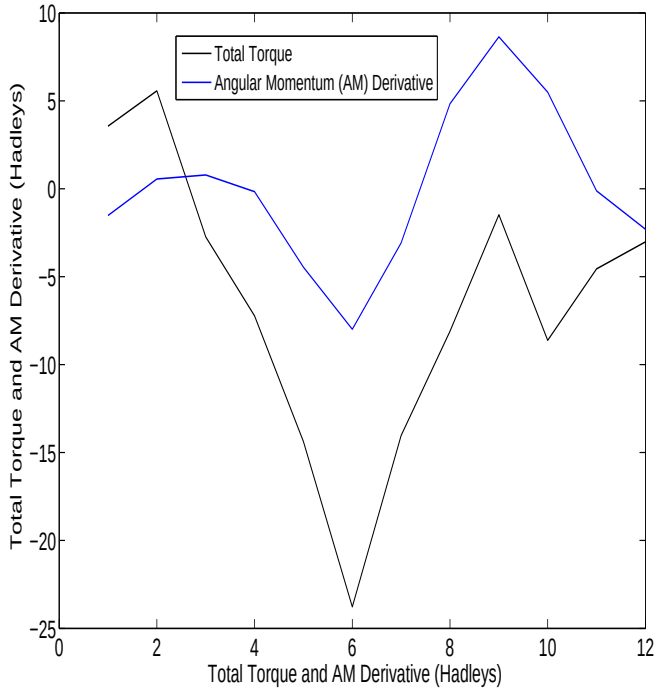

Figure 7.9: Yearly Average Angular Momentum Tendency and Total Torque for 1976-1990

7.1.2 Latitudinal Profiles of the Reanalysis Observation Dataset

The latitudinal profiles calculated allow us to see the (average monthly) contribution to the torque at each latitude over two decades: 1890-1899 and 1990-1999, giving us extra insight into the processes involved. They allow us to see that whether the torques we have seen in the timeseries not only have the right value when summed up over the globe, but whether the datasets' processes are physically correct and generate torques where they should. Taking profiles for two decades also tells us about their dependence on the resolution network required to produce accurate torques.

The mountain torque profile shows good agreement with the profile of Madden and Speth (1995), shown in figure 3.3, in size and shape, with the exception of a sharp peak which is the largest value appearing in the graph, yet is non-existent in Madden and Speth's investigation - we do not know of the cause of this, and whether the NOAA reanalysis is more accurate, or the dataset Madden and Speth analysed is more accurate. We see the presence of the Andes in the southern hemisphere removing angular momentum from the atmosphere, and likewise the himalayas and rocky mountains doing the same in the northern hemisphere. The mountain torque profiles over the two different decades are very similar, suggesting little dependence of the mountain torque on the resolution

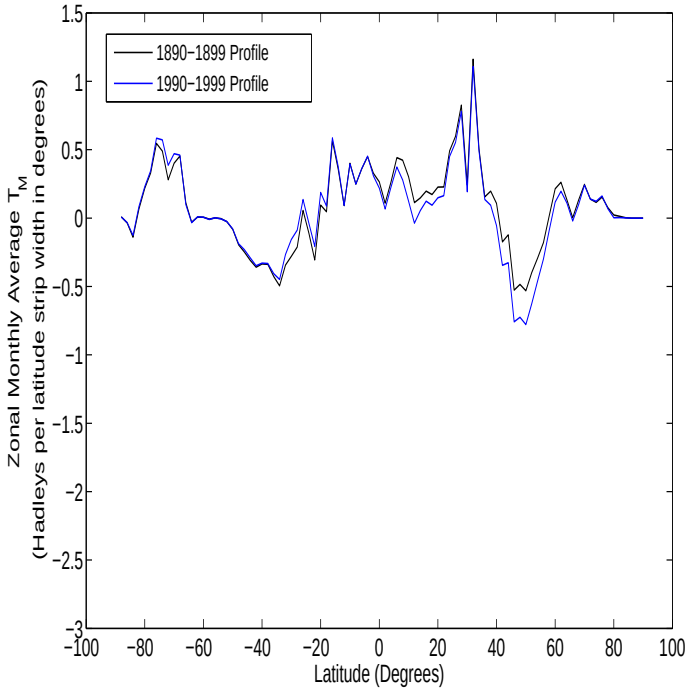

Figure 7.10: Reanalysis Dataset Latitudinal Mountain Torque Profiles for 1890-1899 and 1990-1999

of the observation network, however, there is one exception of slightly more negative values around the northern midlatitudes where the rocky mountains and the himalayas are situated in the 1990-1999 latitudinal profile.

The 10 year average monthly latitudinal friction torque profile reveals the exact same shape in Madden and Speth (1995) that we discussed in section 4.1.1, whilst the values in this dissertation are larger. The values are significantly larger for both the maximums and minimums in this reanalysis dataset, however because Madden and Speth proposed that their friction torque had a large negative bias we should not treat the size of the values associated with the friction torque as a reliable benchmark. There is little difference again between the reanalysis datasets latitudinal friction profile over 1890-1899 and 1990-1999 again suggesting that a poor observation network, with the aid of reanalysis, can produce the same friction profile as today's observational network.

The 10 year average monthly latitudinal gravity wave torque profile shows large contributions in the region of 20°N - 60°N, which is where we see the largest mountain torque activity. This is what we would expect, as the areas of largest mountain torque activity will be where there are significant mountain ranges, and thus there will be significant subgrid scale mountain torque that is not given by the mountain torque calculation but

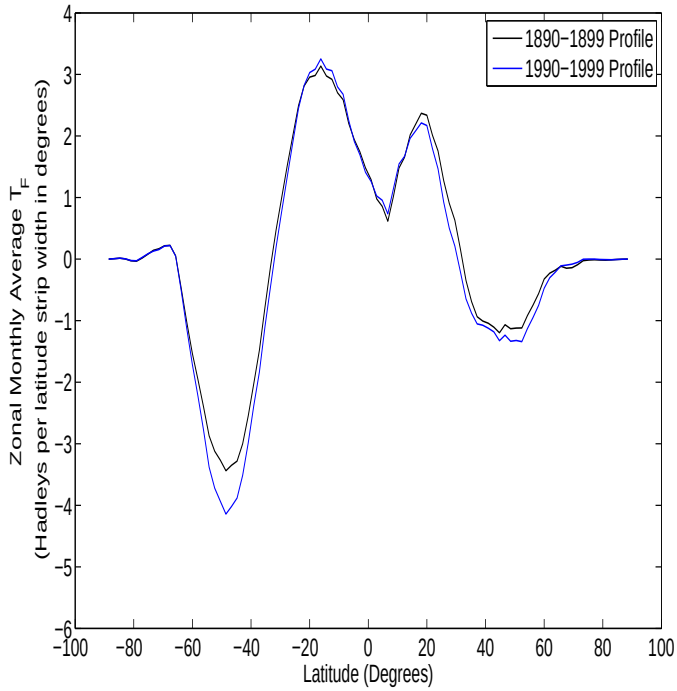

Figure 7.11: Monthly Average Reanalysis Dataset Latitudinal Friction Profiles for 1890-1899 and 1990-1999

needs to be given by the gravity wave torque instead. The values of NOAA's reanalysis gravity wave torque profile generally don't exceed those of the mountain torque, and we would expect the large scale pressure systems and mountains to be more significant than the mountains on subgrid scales. There is little change between the gravity wave torque over the two decades, which suggests that here our gravity wave parameterization used in the reanalysis dataset is not sensitive to changes in the grid resolution of the observation network either. The little change over time with the mountain torque and friction torque profile suggests that there is consistency over time in the results seen, and because the gravity wave torque is the part of mountain and friction torque that is too small to be resolved by Global Circulation Models this perhaps is not unexpected that the gravity wave torque is rather similar over the two decades.

Following on from the idea that there seemed to be large torques in the reanalysis dataset during the northern winter we took two friction profiles, one the average profile over the months december to march during 1990-1999, and one during april to november to see if we could deduce the different processes and differences in circulation between the winter/spring and summer/autumn.

We plot the latitudinal profile from all months over 1990-1999, the winter/spring lati-

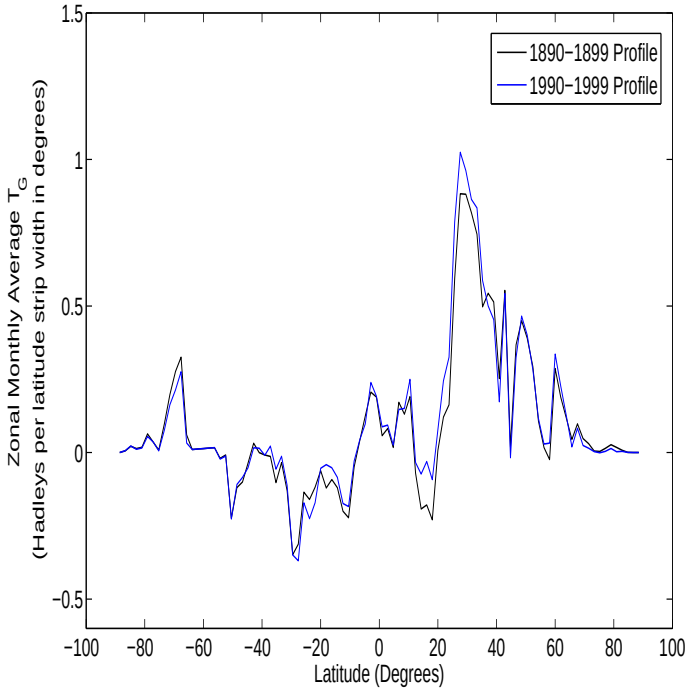

Figure 7.12: Monthly Average Reanalysis Dataset Latitudinal Gravity Wave Torque Profiles for 1890-1899 and 1990-1999

tudinal profile and the summer/autumn latitudinal profile in the following graph.

We see that the values of friction torque in the northern hemisphere equatorial regions are larger during the northern hemisphere winter/spring period than the yearly average or summer/autumn values in the same region. However, this should happen, as the winds throughout the northern hemisphere will be stronger during the northern hemisphere winter as shown in Peixoto and Oort (2007) (also recall our discussion of the increased northern hemisphere jet streams during the northern hemisphere winter in section 3.2, for example). Therefore we see nothing that is seriously erroneous, i.e. there is nothing occuring in the friction torque that should not, and thus it appears that there is just an overestimation of the friction torque over all months comparison to Egger et al. (2007), in particular in the northern hemisphere winter, without serious error to the global circulation patterns the observation dataset.

7.2 Had CM3 Latitudinal Torque Profiles

The torque profiles of HadCM3, and indeed all the climate models, gives us a glimpse into the performance of the climate models, not in predicting specific weather events, but (by

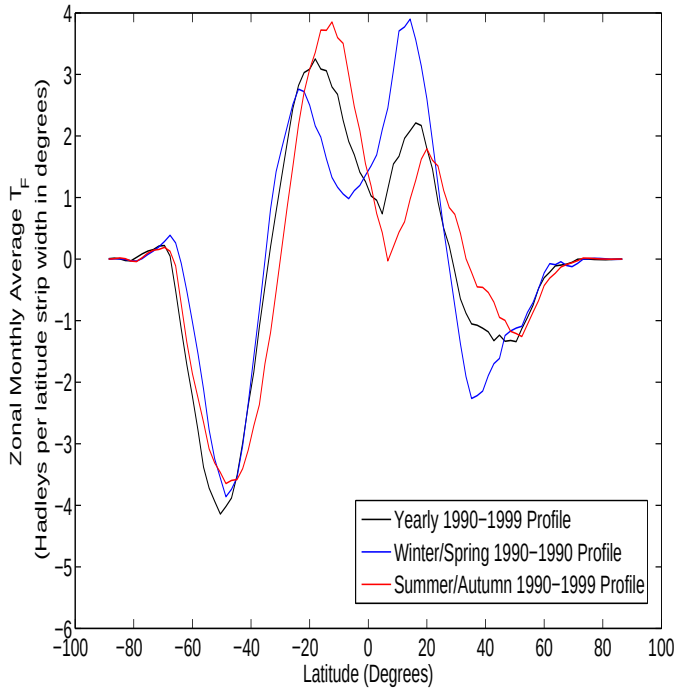

Figure 7.13: Reanalysis Latitudinal Friction Profiles for the whole year, the northern hemisphere winter/spring and the northern hemisphere summer/autumn

taking averages from those weather events in the model) we extract information about the model's physics, and representation of pressure systems, say. Taking the latitudinal profiles of the torques over from two different decades allows us to see into the internal physics for the climate models.

The latitudinal profile of the mountain torque for the Had CM3 is very different to that seen in either in the research undertaken here or in previous investigations such as Madden and Speth (1995). The major region of negative mountain torque is roughly 10°-30° N, whilst negative mountain torque in the southern equatorial regions seems to be accentuated greatly in comparison with what we see in any of the other graphs, or in Madden and Speth (1995).

The Had CM3 model is the coarsest dataset that we study here. Seen as the height fields are invariant, and there is no doubt that these will be accurate, the error in the mountain torque must then lie in one of two, or a combination of the two, places: 1) the numerical calculation we performed on a coarse numerical grid (and yet the model physics and weather representation remains good due to sound subgrid scale representation processes in the model) or 2) the surface pressure values themselves, hence the pressure systems, and thus the weather processes. The lack of change over the two decades tells us

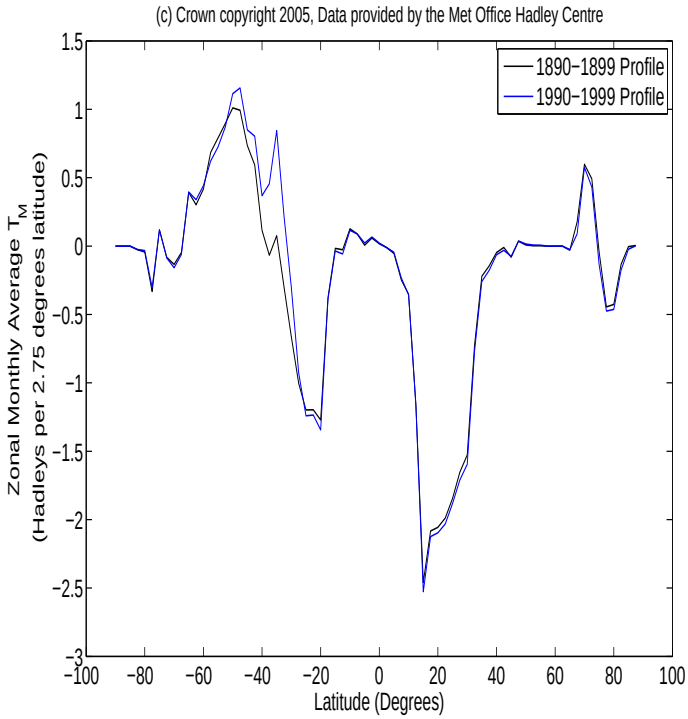

Figure 7.14: HadCM3 Latitudinal Mountain Torque Profiles for 1890-1899 and 1990-1999

that this is not a passing error in the model, and that there is little to no visible model drift in the pattern of its simulated pressure systems - indeed the HadCM3 model has been seen to perform well with regards to little model drift, requiring no periodic adjustment to avoid excessive model drift, as is mentioned in Johns (2003). As mentioned, HadCM3's grid spacing is the worst of all datasets here, and the reanalysis observation dataset and HadGEM1 have grid spacing with roughly twice the number of points on each latitude circle (an imaginary circle, of all longitudes, around the surface of the earth of constant latitude). This is particularly important to note as computation of the mountain torque requires the calculation of a derivative of surface height with respect to longitude - as mentioned earlier Weickmann and Huang (2008) noted the importance of getting the derivative in this equation right to have a correct mountain torque.

A profile of the *reanalysis* observation dataset was taken where the resolution was reduced to half its original value in both latitude and longitude to resemble the grid spacing of HadCM3 by ignoring all points at every other latitude circle, and every other longitude circle on the grid. The profile is shown in figure 7.15.

The largest peak in the original reanalysis profile, around 20°-40°, is shown clearly with roughly similar values, and the himalayas, and rocky mountains still show contributions

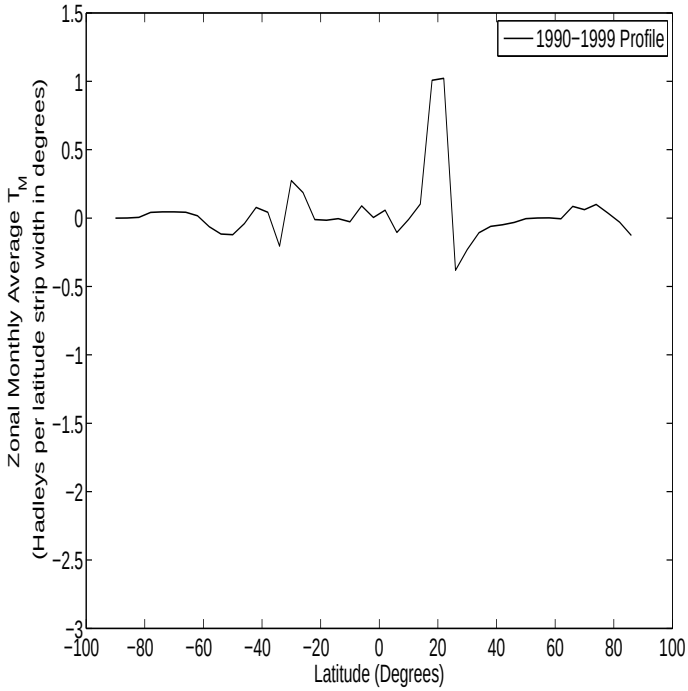

Figure 7.15: NOAA Reanalysis Obervation Dataset Latitudinal Friction Profile 1890-1899 calculated with half resolution

but with smaller, in magnitude, values. The derivative term in the mountain torque is the most problematic of the numerical approximations we take, and although the considerable reduction in detail between the original reanalysis mountain torque profile and the half resolution reanalysis mountain torque profile suggests that there could be a sizeable error in the HadCM3 mountain torque profile due to the grid spacing, the HadCM3 mountain profile cannot be explained completely, or mostly, by the grid spacing. The large negative values in HadCM3 in the northern hemisphere appear to be shifted equatorwards by around 15° in comparison to the reanalysis dataset and the mountain profile of Madden and Speth (1995), and the very large values of the HadCM3 mountain torque latitudinal profile furthermore suggest model error. Whilst not in a journal article, Sea Level Pressure anomalies particularly in North America and the North Atlantic have been reported in HadCM3, by Sutton in 2005 during a joint workshop between the Hadley Centre and the Coupled Ocean-Atmosphere Processes and European Climate (COAPEC). It is beyond the scope of this dissertation for an in depth analysis of the HadCM3 model and journal papers in this area could not be found. However, what must be noted is that the mountain torque, and hence pressure systems, do have non-negligible error - the height fields (which are the other variable in the mountain torque) are time invariant, and undoubtedly reliable.

The difference in the HadCM3 mountain torque profile over the two decades is very little suggesting little change in the pressure systems.

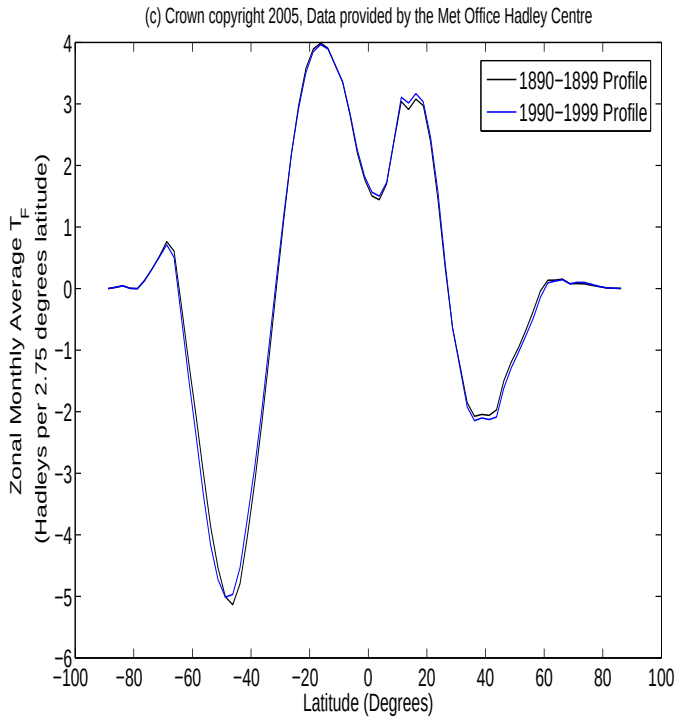

Figure 7.16: HadCM3 Latitudinal Friction Torque Profiles for 1890-1899 and 1990-1999

HadCM3's friction torque latitudinal profile shows a friction profile with values in the expected range that remains invariant over the two decades. It's values are quite large, indeed larger than that of the reanalysis observation dataset, suggesting perhaps one of, or a combination of, stronger winds and a higher land/ocean surface drag coefficient used for the friction stress in the model.

7.3 HadGEM1 Latitudinal Torque Profiles

The HadGEM1 mountain torque latitudinal profile is significantly more like that of the reanalysis dataset and Madden and Speth (1995) than the HadCM3's mountain torque profile. Its values are in the correct range and match very closely to that of the reanalysis dataset, showing the effect of high pressure systems on the west side of the Rocky Mountains, and the Himalayas, and the Andes. As is included in chapter 5 it has a grid that is approximately as fine as that of the reanalysis observation dataset, which will no doubt help in terms of added detail to the torque, and there is little change over the profiles taken from the two different decades.

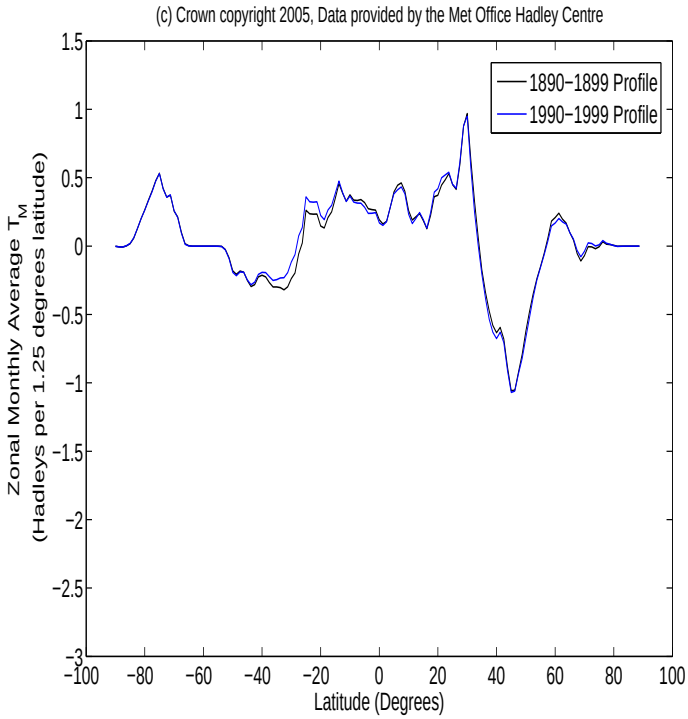

Figure 7.17: HadGEM1 Latitudinal Mountain Torque Profiles for 1890-1899 and 1990-1999

HadGEM1's friction torque, again, is incredibly similar in shape with all friction profiles seen before, and it is almost totally invariant over time. Comparing with the other results we note it's values are smaller than the values seen in the reanalysis observation dataset and HadCM3. It is very interesting to note, in particular, that it's values are smaller than that of the HadCM3 climate model because the models are produced both by the same climate institute, and are very likely to be similary constructed because the HadGEM1's model physics is constructed heavily from HadCM3 (as can be seen at http://www.nec-ug.org/documents/NUG_XVI/NUGXVI_C_Durman.pdf which is a online report by the Hadley Centre about the HadGEM1 model). It is unlikely that the drag coefficient in one model would be double that of another, especially given they come from the same research institute, and it appears that the values of the simulated surface winds in the HadGEM1 model are too weak.

If we were to assume reasonable angular momentum conservation (thus that the flux through the surface actual changes the angular momentum in the atmosphere) suggests a large difference in the amount of angular momentum transport from the equatorial regions and into the midlatitudes, and thus the large scale circulation of the atmosphere (recall in figure 2.2 and equation (2.27) we discussed how the flux across the surface is equal to

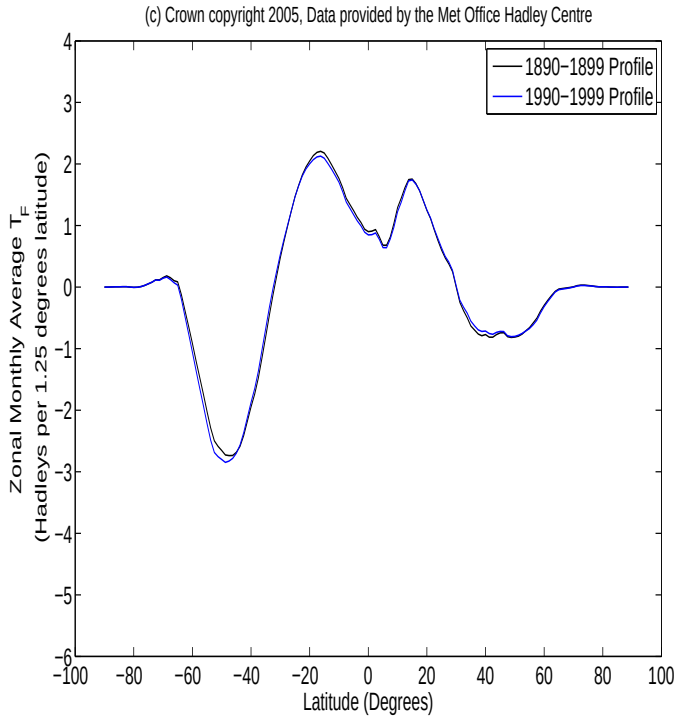

Figure 7.18: HadGEM1 Latitudinal Friction Torque Profiles for 1890-1899 and 1990-1999

the flux across the vertical boundaries). It is particularly exciting to us to note that we can glean such knowledge on the possible differences in the large scale structure and flow through the whole atmosphere in climate models simply from the surface winds.

7.4 NOAA GFDL CM2.0 Latitudinal Torque Profiles

Whilst showing the presence of the andes, the rocky mountains and himalayas, the NOAA GFDL CM2.0 model's mountain torque latitdunial profile is not very similar to the mountain profiles of the reanalysis observation or HadGEM1, or indeed the erroneous profile of HadCM3. The mountain torque profile of the NOAA GFDL CM2.0 is nearly symmetric about the equator. Its grid is slightly more coarse than that of the reanalysis dataset or HadGEM1 however it appears to generate much the same level of detail as that of HadGEM1.

The NOAA GFDL CM2.0's friction torque latitudinal profile shows a friction profile with values similar to that of HadCM3, and the values remain invariant over the two decades, suggesting little to no visible model drift in its wind patterns. It's values aren't as large, suggesting perhaps weaker winds, or a lower land/ocean surface drag coefficient used for the friction stress in the model. The friction torque latitudinal profile is also largely

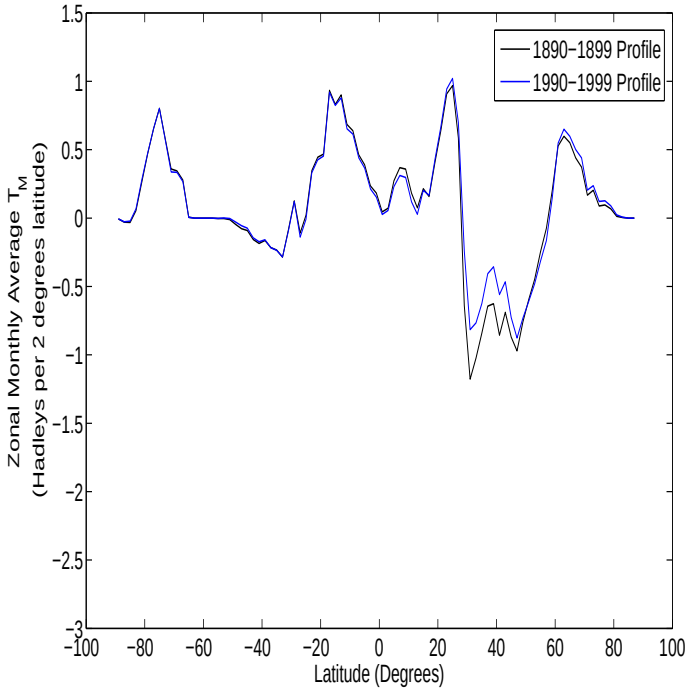

Figure 7.19: NOAA GFDL CM2.0 Mountain Torque Latitudinal Profiles for 1890-1899 and 1990-1999

symmetric, and it's positive peak in the northern hemisphere equatorial regions along with its near symmetric mountain torque suggests the circulation is almost symmetric about the equator, i.e. the circulation of the whole atmosphere is nearly the same in the north and south hemispheres in the NOAA GFDL CM2.0 model, this is not true in the real atmosphere.

As the friction torque latitudinal profile of HadGEM1 has values about 1.5 to 2 times less than that of the all the other climate models we have now seen it is suspected that it has weaker winds than the other models. Of course, the implications of this affect the whole circulation in the HadGEM1 model.

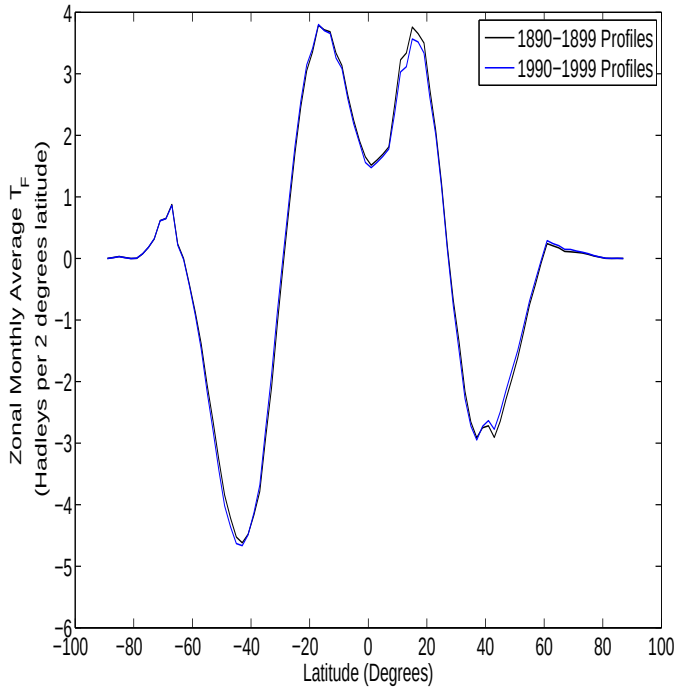

Figure 7.20: NOAA GFDL CM2.0 Friction Torque Latitudinal Profiles for 1890-1899 and 1990-1999

Chapter 8

Conclusions and Further Work

8.1 Summary

We conclude that the NOAA Reanalysis Observation dataset, like many others, does not conserve angular momentum. It is thought that the error lies almost completely in the torques and that any error in the angular momentum is negligible. It is believed that major error lies in the gravity wave torque in the northern hemisphere winter (and that the choice of the gravity wave torque parameterization is not the main factor), along with the friction torque, which exhibits a large positive bias over all times (but particularly in the northern hemisphere winter), and also the mountain torque which, too, shows a large bias over the northern hemisphere winter. We note that there seems to be some large error coming from the data assimilation process, however, we are not able to pinpoint the cause(s).

Furthermore, the significant decrease in the friction and mountain torques over 1961-1990 causes a negative shift in the total torque over time which further contributes to a lack of conservation of angular momentum. Thus it is, as with Madden and Speth (1995), that a loss of total torque contributes to the lack of conservation of angular momentum and not the values of angular momentum.

The total average monthly torque is -3.8 Had, and indeed the fact that sometimes the total torque exceeds the angular momentum tendency suggests that there is a better yearly balance between the torques and angular momentum tendency than in Madden and Speth (1995). Despite the poor performance the dataset does however show many fundamental features of larger angular momentum during the northern hemisphere winter months and lower angular momentum summer months associated with speeding up and slowing down of the jet streams.

Moreover, the little change in the latitudinal torque profiles in the reanalysis observation dataset suggests that with the aid of the reanalysis process a very poor observation

network can give the same latitudinal torque profiles as the observation network of today.

The climate models do show some promising features in their latitudinal profiles of the torques. Little change over time in the torques, and hence pressure systems, wind strengths and patterns, and so on, suggest consistency in the models with little serious model drift. However we see a clear difference in the HadCM3 model's mountain torque profile, and that of all others in this, and other, research. Further where this model repeats this pattern over both decades suggests that it is not just a passing anomaly, but a good reflection of the internal model physics. The mountain torque and friction torque of the NOAA GFDL CM2.0 climate model, were invariant over time, suggesting no visible drift. The mountain and friction torque profiles were almost symmetric about the equator suggesting that the atmosphere, as simulated in the model, is in a circulation pattern that is symmetric about the equator.

Whilst no datasets had identical latitudinal friction profiles, perhaps the most interesting difference in the friction profiles was between the Hadley Centre HadCM3 and HadGEM1 models - with the values in one model being twice the size of the other. We found this particularly interesting because the models are made by the same institute and are likely to have been constructed in a similar manner. We noted that the differences in sizes is most likely to be attributable to the wind speeds simulated in the models, and that HadGEM1 seems to have weaker surface winds than any climate model or observation dataset in this investigation. Also assuming reasonable angular momentum budget conservation in the models the difference in flux of angular momentum into the equatorial regions would have large scale applications for the atmospheric circulation the models.

8.2 Further Work

8.2.1 Torques and the Northern Hemisphere Winter in the NOAA Reanalysis Observation Dataset

Due to the lack of conservation of angular momentum, one recommendation from this dissertation is to investigate the causes of the erroneous torque values during the northern hemisphere winter in the reanalysis observation dataset. The idea of identifying the cause of such time dependent anomalies in the torques directly calls for the use of covariance analysis of the angular momentum and torques. This would allow us to glean the time dependent contributions and activity between the four variables (angular momentum, mountain, friction and gravity wave torque) that are associated with the atmospheric angular momentum budget.

Essentially the time covariances of the terms measure of how much two variables change together over time.

We take these ideas from Egger and Hoinka (2002) who sought to understand the time dependent links between the torques and angular momentum in relation to the angular momentum conservation equation (2.29). This time dependent analysis comes from looking at the covariance terms of the torques and angular momentum, and comes from analytic manipulation of the equation (2.29).

The expectation of a time series is the value/outcome that you would expect to see on average, and is given by

$$E(X) = \sum_i x_i p(x_i) \tag{8.1}$$

and if we multiply equation (2.29) by $M(t-\tau)$ and take expectations then we get

$$\frac{d}{d\tau} C(M; M|\tau) = C(M; T_M|\tau) + C(M; T_F|\tau) + C(M; T_g|\tau) \tag{8.2}$$

Note the covariance functions are $C(x_i; x_j|\tau) = E[x_i(t)x_j(t+\tau)]$, where $x_1 = M$, $x_2 = T_M$, $x_3 = T_F$, $x_4 = T_G$.

We may extract the time dependent behaviour of the torques and angular momentum and their links and contributions to each other in the dataset through this method.

Moreover, Egger et al. (2003) furthered the covariance analysis, and angular momentum conservation work by Egger and Hoinka (2002) by noting that if we subtract the two angular momentum tendency equations from each other we get

$$\frac{d\Delta M}{dt} = \Delta T_M + \Delta T_f + \Delta T_g \tag{8.3}$$

and that a similar covariance analysis can be made to understand the time dependent differences in torques (aswell as conservation) between two datasets to understand their physical consistency and agreement. This could be of use to us in discovering differences between the physics of the torques in the NOAA reanalysis dataset, and another reanalysis dataset, say ERA-40 (which is a dataset that includes a gravity wave stress parameterization already calculated and has been tested far more extensively than the NOAA model).

For equation (8.3) they noted a few possibilities

1. That neither observation dataset would satisfy conservation of angular momentum equation, equation (2.29).

2. That each dataset would satisfy conservation of angular momentum equation, equation (2.29), individually, but they would not satisfy equation (8.3), that is that they are internally consistent in their conservation of angular momentum, but they have different realities.

3. That they satisfy both the conservation of angular momentum equation, equation (2.29), and they satisfy equation (8.3), i.e. the size of the torques and angular momentum, and the duration of torque and angular momentum events (and thus weather events) are the same.

Indeed, during this intercomparison perhaps a power spectrum of the difference between the angular momentum would tell us the difference in response and disparity between activity of the datasets. It would be pleasing for 'completeness' to have an analysis for the whole time the dataset has been run for, however this would be considerable computationally expensive.

8.2.2 Conservation of Angular Momentum on the Climate Models

Calculations of angular momentum and torques for the three climate models would be one of the next things to investigate. This would allow us to test the conservation of angular momentum on the climate models aswell. We could then establish the internal realism of the model physics - indeed, it could be that despite the HadCM3 model's erroneous mountain torque it is actually internally physically realistic and it conserves angular momentum! Indeed angular momentum could be tested on many more of the 25 climate models in the WCRP's CMIP3 mutli-model database.

It may be wise to look at the time dependent interactions of the torques and angular momentum in climate models aswell. To understand the applicability of testing our Climate Models to the previous covariance analysis we suggested we note that in their paper, Egger et al. (2003), whilst taking an intercomparison between the two reanalyses datasets, are effectively discussing the differences in accurate representation of specific weather events between two observation datasets. However we cannot hope to apply their analysis associated with equation (8.3) and the resulting covariance analysis from equation (8.3).

Due to the chaotic nature of the atmosphere not even a numerical weather prediction model could accurately predict events a few weeks ahead, so, unlike the source of difference between reanalyses observation sets which may be primarily linked with data assimilation errors, the difference in Climate Models, which have a much poorer resolution, will be from the fact that they simply aren't capable of predicting weather events.

Moreover, even if such models were somehow capable of doing so, climate models, generally, are 'spun-up' into a representative state of the Climate at a certain time instead of started from initial conditions at a certain time, so the covariance analysis used by Egger et al. (2003) is not at all suitable for Climate Model comparison - Climate Models' specific MJO's and ENSO's will be of differing time lengths and strengths to the actual MJOs and ENSOs. What is important is that they represent processes and events *statistically* well,

so the way to compare climate models would be based on the statistical averages of their events.

However, we note that it is appropriate to follow the analysis of Egger and Hoinka (2002) by applying the covariance analysis associated with equation (8.2) to a climate model to see if it is *internally* realistic.

8.2.3 The HadCM3 Mountain Torque

Another recommendation from this project is to investigate the causes of the Had CM3's mountain torque. Whilst it was shown that calculating a latitudinal mountain torque profile on a coarser numerical grid can change the latitudinal profile, the error seen in HadCM3's latitudinal mountain torque profile cannot be attributed to a sparser grid: particularly the significantly larger values seen in the HadCM3 mountain torque profile than any other latitudinal mountain torque profile, and the significant contributions from regions closer to the equator than in Madden and Speth (1995), the reanalyses observation set, HadGEM1, and NOAA GFDL CM2 show that there is significant error in the pressure systems of the model itself.

8.2.4 The HadCM3 and HadGEM1 Friction Torques

The difference between the HadCM3 and HadGEM1 friction torques should be investigated. We suggested that the difference in the sizes of the friction torques mean that the models could have a large difference in the strengths of their atmospheric circulation. Initially we should look at attributing the causes of the difference in sizes of the friction torques through looking at the wind speeds and also, to be certain, the surface drag coefficients. If we calculated angular momentum (as suggested above) and the models conserve angular momentum reasonably well then this difference in friction torque will have large implications for the transfer of the atmospheric angular momentum and the circulation in the atmosphere. Once angular momentum budget studies have been performed we could investigate the zonal average angular momentum transport through the atmosphere, details of which are explained extensively in Peixoto and Oort (2007), to discern differences in the atmospheric circulation.

8.2.5 Raised Lid Hadley Centre Climate Models, Radiative Peturbation, Angular Momentum Conservation and Gravity Wave Parameterization

Some Hadley Centre Climate Models have just had their model lid height (the maximum height of the atmosphere represented in the model) increased from 40km to 85km. Impor-

tant work is being done on these models such as contribution of results to the next IPCC report. Specifically projects are being conducted to test the responses of climate models to volcanic eruptions in the research project "Stratospheric Particle Injection for Climate Engineering" (see the Stratospheric Particle Injection for Climate Engineering (SPICE) Project Website: http://gow.epsrc.ac.uk/ViewGrant.aspx?GrantRef=EP/I01473X/1).

In their paper, Shaw and Sheperd (2007), note that subject to radiative peturbation in the middle atmosphere the climate model response can be trustworthy or not. With angular momentum conservation and a range of gravity wave parameterizations the response of the climate models tested to this radiative peturbation is robust to changes such as the model lid height. However, when angular momentum is not conserved, due to the formulation or implementation of the gravity wave torque parameterization, there is a "non-negligible" spurious response from the imposed middle atmosphere radiative peturbation when the climate model lid height is changed. Further work into testing the conservation of angular momentum with the new raised lid models and investigations into their gravity wave torque parameterizations could be investigated as to whether this spurious response will occur in the model, contributing unreliable results to the project.

***

With knowledge of angular momentum theory and the code for calculating angular momentum, which can be easily modified for use any model, and also values for the NOAA reanalyses dataset's angular momentum already at hand, a lot of these projects could be acheived quickly with large computing power. The gravity wave drag experiment could, potentially, be a much longer investigation.

Chapter 9

Appendix 1 - Coordinates

The relationship between the spherical unit vectors $\mathbf{e}_\lambda$, $\mathbf{e}_\theta$ and $\mathbf{e_r}$ and the unit vectors in which we express angular momentum, taken from Egger et al. (2007), is shown below

$$\mathbf{e}_\lambda = -\mathbf{i_1}\sin\lambda + \mathbf{i_2}\cos\lambda \tag{9.1}$$

$$\mathbf{e}_\theta = -\mathbf{i_1}\cos\lambda\sin\theta - \mathbf{i_2}\sin\lambda\sin\theta + \mathbf{i_3}\cos\theta \tag{9.2}$$

$$\mathbf{e_r} = \mathbf{i_1}\cos\lambda\cos\theta + \mathbf{i_2}\sin\lambda\cos\theta + \mathbf{i_3}\sin\theta \tag{9.3}$$

Chapter 10

Appendix 2 - Techniques of Computation

There is significantly more than just a choice of numerical approximation when choosing how to compute the angular momentum and torques because the choice of what to use to calculate the torques and angular momentum has a physical meaning.

Although it does not change our analysis, it should be noted that we do not strictly test equation (2.29) for all time, but the time averaged version

$$\frac{\partial \overline{M}}{\partial t} = \overline{T_F} + \overline{T_G} + \overline{T_M} \tag{10.1}$$

over a discrete set of values.

Recall the time average over a (time) interval $[0, \tau]$ of a variable A as

$$\overline{A} \equiv \frac{1}{\tau} \int_0^\tau A dt \tag{10.2}$$

10.1 Angular Momentum

We can calculate angular momentum from equation (2.12), however, this requires estimates of the density of the atmosphere over the whole of the atmosphere. Estimating the density over the atmosphere is notoriously hard, and to avoid this problem angular momentum can be written as

$$M = M_\Omega + M_r = \frac{a^4 \Omega}{g} \int_{10}^{1000} \int_{\lambda=0}^{2\pi} \int_{\theta=-\pi/2}^{\pi/2} p_{sfc} cos^3\theta d\theta d\lambda + \frac{a^3}{g} \int_{10}^{1000} \int_{\lambda=0}^{2\pi} \int_{\theta=-\pi/2}^{\pi/2} u cos^2\theta d\theta d\lambda dp \tag{10.3}$$

as is done by Madden and Speth (1995). This reduces calculating angular momentum

to a surface integral and a volume integral involving the u-wind component over pressure levels and liberates us from attempting to estimate density in the whole atmosphere. The angular momentum is integrated not over the whole atmosphere, but over the volume of atmosphere bounded by the surface and the 10hPa Pressure Level (as has been done in Madden and Speth (1995) and other angular momentum investigations) because of the restrictions on model height, however, the error from this 10hPa limit is not too large.

10.2 Friction Torque

Note for the forthcoming discussion that the 'momentum flux' we talk of here is the force per unit area or friction stress in the east west direction. Friction Torque has been previously calculated by taking direct observations of the turbulent fluxes near the ground, or on bulk formulations for the momentum fluxes near the ground, however, it is significantly more common that bulk formulations are used than direct observations. As bulk formulations are not based on observed reality they have been tested extensively at ocean buoys in homogeneous terrain, however there are extensive uncertainties above complex terrain Egger et al. (2007). Egger et al. (2007) also point the comment made by Ponte and Rosen (2001) that estimates of the uncertainties of these bulk formulations are not available.

Weickmann (2003) discussed the use of a stochastic friction torque, whilst Egger (2005) modified the stochastic model by Weickmann et al. (2000) which included stochastic torques and angular momentum.

The friction stress τ_F may be obtained from the observation dataset directly, or this data can be put in a forecast model, and then the data for the friction stress can be calculated from this. This is what Madden and Speth (1995) do (specifically they obtain the friction stress at time 0000 by averaging the surface stress from the forecast model over the 12 hour period from 1800-0600). The assumed advantage of using the forecast model over the observed data is that the forecast model parameterizations includes vertical stability aswell as wind values, Madden and Speth (1995).

For the numerical approximation the obvious and most simple approximation to choose is

$$T_F = R^3 \int \int \tau_F cos^2\theta d\theta d\lambda \approx R^3 \sum_i \sum_j \tau_F^{i,j} cos\theta_j \Delta\theta_j \Delta\lambda_i \tag{10.4}$$

10.3 Mountain Torque

In analysing the global angular momentum balance in reanalyses observation datasets and climate models it is essential we have a good numerical scheme for the computation of mountain torque because of its derivative term, as has been discussed by Weickmann and Huang (2008).

Mountain torque has been calculated by taking height and surface pressure in a fourier series at each latitude as done by Madden and Speth (1995) on a spectral model. Spectral models are a different type of model that represent the climatic variables over the globe without using grid points, however we shall not go into more detail on these models here. However, using this type of model the fourier series for the height was then differentiated with respect to λ, and its coefficients were multiplied by those of the surface pressure to give zonal averages, before mountain global torque is calculated. As with friction torque, Weickmann (2003) investigated the Stochastic Representation of Mountain Torque.

Weickmann and Huang (2008) talk about the computation of mountain torque from gridded global datasets, and compare the mountain torque of numerical finite difference schemes to the spectral method's calculation of mountain torque (note this is *not* the same as using a spectral model). The reason for their investigation is that whilst the spectral method is highly accurate it is also comparatively computationally expensive, and to understand the conclusions they came to we will go follow their steps. Thus consider the formula for the mountain torque

$$T_M = a^2 \int_{-\pi/2}^{\pi/2} Y_M cos\theta d\theta \tag{10.5}$$

where the inner integral is

$$Y_M = \int_0^{2\pi} X d\lambda \tag{10.6}$$

and where $X = -(p\Delta h)/(\Delta\lambda)$ or $X = (h\Delta p)/(\Delta\lambda)$. They note the integration of equation (10.5) is a simple matter, and they are concerned more with the inner integral approximation involving a derivative of pressure, or height, with λ. Here they suggest the approximation

$$Y_M = \int_0^{2\pi} X d\lambda \approx \sum_i^N X_i \Delta\lambda \tag{10.7}$$

where $\Delta\lambda = \frac{2\pi}{N}$. They note that whilst this is a simple approximation it gives the same value of for whichever line of longitude ones start the integration at, meaning thus that the results are not influenced and distorted by the position that one starts the integration.

Then for

$$X_i = -p_i \left(\frac{\partial h}{\partial \lambda}\right)_i \tag{10.8}$$

they study six finite difference schemes

$$\left(\frac{\partial h}{\partial \lambda}\right)_i = \frac{1}{\Delta\lambda} \sum_{k=-K}^{k=K} b_k h_{i+k} \tag{10.9}$$

Any finite difference approximation to the derivative may be split into two classes, centered (i.e $b_{i+k} = -b_{i-k}$ for $k = 1, 2, ..., M$) and non-centered (any scheme that is not centered). Thus $b_{-1} = -1/2$, and $b_1 = 1/2$, with all other b_i's equal to zero, is a centered difference scheme, and $b_{-2} = 1/2$, $b_{-1} = -2$, $b_0 = 3/2$, with all other b_i's equal to zero is a non-centered scheme.

The six schemes they test in a comparison to the spectral method will not be written here, however can easily be seen in their paper. Weickmann and Huang note that the noncentered schemes effectively shift the mountain orography, and thus will render the essentially important pressure/mountain location relation highly inaccurate. They advise that such a noncentered finite difference scheme should never be used in angular momentum budget studies. Indeed, the unreliability of the non-centered schemes is exhibited when they see that the mountain torque from the third order scheme is significantly worse than that from the second order scheme!

However, the centered schemes are deemed to be a good approximation. The second, fourth and sixth order centered schemes converge rapidly to the solution given by the spectral method as the order increases.

Centered schemes, they point out, do, however, have a tendency to damp the derivative and so actually predict the mountain to be lower than it is. This makes some mountains less steep in their computation than they are in real life, and thus there will be an over or under, depending on typical location of pressure systems around mountain regions, estimation of mountain torque in that region. This is a particular cause of error for the approximation of the mountain torque in the Andes, which is a long and narrow, but steep, mountain range.

Recalling that the mountain torque can be written in two equivalent forms, Weickmann and Huang write out the approximation for the second integral form, given already in equation (2.33). For the two integrals to be equal, one *requires* that

$$Y_{M,1} = Y_{M,2} \tag{10.10}$$

where $Y_{M,1} = -\mathbf{p}^T \mathrm{Q} \mathbf{h}$, and $Y_{M,2} = \mathbf{h}^T \mathrm{Q} \mathbf{p}$, ($\mathbf{h}$ is the vector of height and $\mathbf{p}$ is the

vector of surface pressure and Q is the matrix of coefficients resulting from the b_i chosen in the finite difference scheme).

Thus they look at

$$Y_{M,2} - Y_{M,1} = \mathbf{p}^T \mathrm{Q}\mathbf{h} + \mathbf{h}^T \mathrm{Q}\mathbf{p} \tag{10.11}$$

which can be written as

$$Y_{M,2} - y_{M,1} = \mathbf{h}^T (\mathrm{Q} + \mathrm{Q}^T)\mathbf{p} \tag{10.12}$$

and, Weickmann and Huang (2008) note that this is zero if $\mathrm{Q} = -\mathrm{Q}^T$, i.e. Q is antisymmetric. An encouraging find is that this is true for all centered difference schemes, whilst they note that the non-centered schemes do not satisfy this property.

10.4 Gravity Wave Torque

We may take the values of the gravity wave stress from the model directly, or from the forecast values, in much the same way we did for friction stress.

Gravity Wave Torque has been studied much less over history, and the parameterizations that have been employed do not have much observational backing, as mentioned in Egger et al. (2007).

Numerically the same approximation may be taken for the gravity wave torque as the friction torque.

i.e.

$$T_G = R^3 \int\int \tau_G cos^2\theta d\theta d\lambda \approx R^3 \sum_i \sum_j \tau_G^{i,j} cos\theta_j \Delta\theta_j \Delta\lambda_i \tag{10.13}$$

Chapter 11

Bibliography

Acheson, D. J., 1990. Elementary Fluid Dynamics. 2006 Reprint. New York, Oxford University Press.

Compo, G.P., J.S. Whitaker, P.D. Sardeshmukh, N. Matsui, R.J. Allan, X. Yin,B.E. Gleason, R.S. Vose, G. Rutledge, P. Bessemoulin, S. Brnnimann, M. Brunet, R.I. Crouthamel, A.N. Grant, P.Y. Groisman, P.D. Jones, M.C. Kruk, A.C. Kruger, G.J. Marshall, M. Maugeri, H.Y. Mok, Ø. Nordli, T.F. Ross, R.M. Trigo, X.L. Wang, S.D. Woodruff, S.J. Worley, 2009: The Twentieth Century Reanalysis Project. Quart. J. Roy. Meteor. Soc., submitted.

Compo, G.P., J.S. Whitaker, and P.D. Sardeshmukh, 2006: Feasibility of a 100 year reanalysis using only surface pressure data. Bull. Amer. Met. Soc., 87, 175-190.

Egger, J., and K.-P. Hoinka, 2002. Covariance Analysis of the Global Atmospheric Axial Angular Momentum Budget. Monthly Weather Review, 130, 1063-1070.

Egger, J., and K.-P. Hoinka, 2005. The Annual Cycle of the Axial Angular Momentum of the Atmosphere. Journal of Climate, 18, 757-771.

Egger, J., K. Weickmann, and K.-P. Hoinka (2007), Angular momentum in the global atmospheric circulation, Rev. Geophys., 45, RG4007, doi:10.1029/2006RG000213.

Huang, H.-P., P. D. Sardeshmukh, and K. M. Weickmann, (1999). The balance of global angular momentum in a long-term atmospheric data set. J. Geophys. Res., 104, 2031-2040.

Johns, T. C. 2003. Anthropogenic climate change for 1860 to 2100 simulated with the HadCM3 model under updated emissions scenarios. Climate Dynamics 20:583612.

V. Lucarini: "Validation of Climate Models". This is a contributed article (pages 1053-1057) in: Ed. G. Philander, 2008. Encyclopedia of Global Warming and Climate Change. SAGE (Thousand Oaks, USA).

Madden, R.A, Speth. P., 1995. Estimates of Atmospheric Angular Momentum, Friction and Mountain Torques during 1987-1988. Journal of the Atmospheric Sciences, 52 (21), 3681-3694.

Meehl, G. A., Covey, C., Delworth, T., Latif, M., McAvaney, B., Mitchell, J.F.B., Stouffer, R.J., Taylor, K.E., 2007. The WCRP CMIP3 multi-model dataset: A new era in climate change research. Bulletin of the American Meteorological Society, 88, 1383-1394.

Oort, A., 1989. Angular Momentum in the Atmosphere-Ocean-Solid Earth System, Bulletin of the American Meteorological Society, 70 (10), 1231-1242.

Palmer, T. N., G. J. Shutts, and R. Swinbank, 1986: Alleviation of a systematic westerly bias in general circulation and numerical weather prediction models through an orographic gravity wave drag parameterization, Quart. J. R. Met. Soc., 112, 1001-1039.

Peixoto, J.P., Oort, A. 2007. Physics of Climate. New York: Springer.

Shaw, Tiffany A., Theodore G. Shepherd, 2007: Angular Momentum Conservation and Gravity Wave Drag Parameterization: Implications for Climate Models. J. Atmos. Sci., 64, 190-203

Sutton, R. Seasonal to Decadal Climate Variability: Analyses using HadCM3. A report of a joint Hadley Centre COAPEC workshop on 22nd-23rd March 2005 at the Met Office, Exeter. Available from http://www.noc.soton.ac.uk/coapec/pdfs/Workshop_4.pdf

Weickmann, Klaus M., George N. Kiladis, Prashant D. Sardeshmukh, 1997: The Dynamics of Intraseasonal Atmospheric Angular Momentum Oscillations. J. Atmos. Sci., 54, 1445-1461

Weickmann, K., 2003. Mountains, the Global Frictional Torque, and the Circulation over the Pacific-North American Region, Monthly Weather Review, 131, 2608-2622.

Weickmann, K., Huang, H.-P., 2008. On the Computation of the Mountain Torque

from Gridded Global Datasets, Monthly Weather Review, 136, 4005-4009.

Weickmann, K.M., Sardeshmukh, P.D. 1994. The atmospheric angular momentum cycle associated with a Madden-Julian oscillation. Journal of the Atmospheric Sciences, vol.51, no.21, p. 3194-208

White, M., 1949. The Role of Mountains in the Angular-Momentum Balance of the Atmosphere. Journal of Meteorology, 6, 353-355.

Whitaker, J.S., G.P.Compo, X. Wei, and T.M. Hamill 2004: Reanalysis without radiosondes using ensemble data assimilation. Mon. Wea. Rev., 132, 1190-1200.

Zharov, V. E., 1996. Connection of the earth's rotation with the atmospheric angular momentum and the strongest earthquakes. Astronomical & Astrophysical Transactions: The Journal of the Eurasian Astronomical Society, 9 (4), 317-327.